Reduced intestinal GLP-1$^+$ cell numbers are associated with an inflammation-related epithelial metabolic signature

Short title: Reduced GLP-1$^+$ cells in gut inflammation

Elisabeth Urbauer[1‡], Doriane Aguanno[1‡], Katharina Kuellmer[2‡], Amira Metwaly[1], Nadine Waldschmitt[1], Mohamed Ahmed[1], Sevana Khaloian[1], Gabriele Hörmannsperger[1], Julien Planchais[3], Tobias Fromme[2,4], R Balfour Sartor[5], Harry Sokol[3,6,7], Dirk Haller[1,8], Eva Rath[1]*

[1]Chair of Nutrition and Immunology, School of Life Sciences, Technical University of Munich, Freising, Germany

[2]Chair of Molecular Nutritional Medicine, School of Life Sciences, Technical University of Munich, Freising, Germany

[3]Micalis Institute, INRA, AgroParisTech, Université Paris-Saclay, Jouy-en-Josas, France

[4]EKFZ-Else Kröner-Fresenius Center for Nutritional Medicine, Technical University of Munich, Freising, Germany

[5]Department of Medicine, Center for Gastrointestinal Biology and Disease, University of North Carolina at Chapel Hill, Chapel Hill, North Carolina, USA.

[6]Sorbonne Université, INSERM, Centre de Recherche Saint-Antoine, CRSA, AP-HP, Saint-Antoine Hospital, Gastroenterology Department, 75012 Paris, France

[7]Paris Center for Microbiome Medicine (PaCeMM) FHU, Paris, France

[8]ZIEL Institute for Food and Health, Technische Universität München, Freising, Germany

* Correspondence: Eva Rath, TUM SoLS, Gregor-Mendel Str. 2, 85354 Freising eva.rath@tum.de

[‡] these authors contributed equally

Disclosures: *The authors declare that the research was conducted in the absence of any commercial or financial relationships that could be construed as a potential conflict of interest*.

Preprint Server: https://www.biorxiv.org/content/10.1101/2025.03.05.641577v1

Word Count: 5.470

Grant support: NIH P40OD01995, P30DK034987, P01DK94779 (RBS), Crohn's & Colitis Foundation (RBS)

Data Transparency: All data generated or analyzed during this study are included in this published article. Additional datasets, including raw data, are available from the corresponding author upon reasonable request.

Synopsis: This study examines GLP-1^{+} cells in intestinal inflammation, showing consistent reductions in inflamed areas. Findings from mouse models and human data reveal an inflammatory metabolic profile linked to altered epithelial differentiation. GLP-1, involved in endocrine-immune crosstalk, may impact mucosal inflammation and symptoms, making it a therapeutic target.

Graphical Abstract:

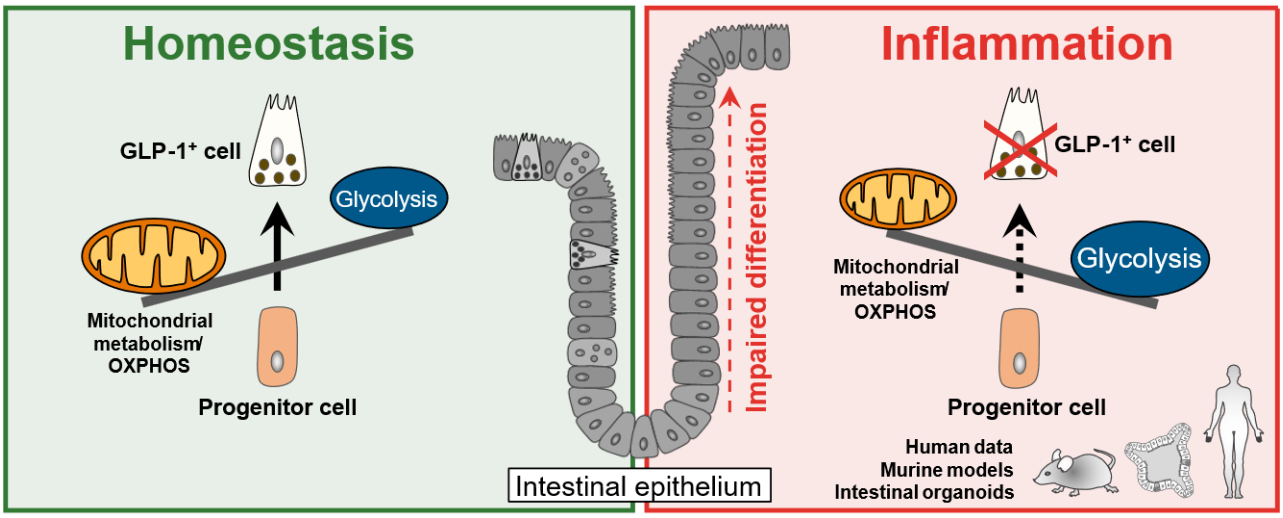

38 Abbreviations:

39	AMPK	5'-prime-AMP-activated protein kinase
40	Atf/ ATF	Activating transcription factor
41	ATP	Adenosine triphosphate
42	Cck/ CCK	Cholecystokinin
43	CD	Crohn´s disease
44	ClpP	Caseinolytic mitochondrial matrix peptidase
45	Dclk	Doublecortin-like kinase protein
46	EEC	Enteroendocrine cell
47	Gcg/ GCG	Glucagon
48	GLP	Glucose like protein
49	Hmgcs2/ HMGCS2	3-Hydroxy-3-methylglutaryl-CoA synthase
50	HS	Histoscore
51	IBD	Inflammatory bowel diseases
52	IEC	Intestinal epithelial cell
53	IL	Interleukin
54	Isl	Insulin gene enhancer protein
55	Mtor	Mechanistic target of Rapamycin
56	Ngn/NEUROG	Neurogenin
57	Pax	Paired box
58	PRKAA	Protein kinase AMP-activated catalytic subunit alpha
59	Pyy/PYY	Peptide YY
60	Rfx6/ RFX6	Regulatory Factor X 6
61	Tnf	Tumor necrosis factor
62	TPH	Tryptophan hydroxylase
63	Trib/TRIB	Tribbles pseudokinase
64	UC	Ulcerative colitis
65	Wt	Wild type

66 **Abstract**

67 **Background & Aims** Enteroendocrine cells (EECs) are known for their role in digestion and
68 metabolism, yet their role in intestinal inflammation remains unclear. In inflammatory bowel diseases
69 (IBD), a contribution of EECs to pathogenesis is indicated by autoantibodies affecting EEC function
70 and general disease symptoms like insulin resistance and altered intestinal motility. Particularly, the L
71 cell-derived hormone glucagon-like peptide 1 (GLP-1), suggested to orchestrate metabolic-
72 inflammatory responses may influence inflammatory pathways in the intestine.

73 **Methods** We quantified numbers of GLP-1^{+} cells in 4 different mouse models of intestinal
74 inflammation and performed transcriptional analyses of colonic epithelial cells from inflamed
75 interleukin (IL)10-deficient mice. Using a publicly available single-cell RNA sequencing dataset
76 including mucosal biopsies from Crohn´s disease (CD) patients, we confirmed findings from the
77 murine models. A model of mitochondrial dysfunction (ClpP$^{\Delta IEC}$ mice) as well as murine and human
78 intestinal organoids were used to study molecular mechanisms.

79 **Results** Numbers of GLP-1 expressing cells are consistently reduced at the site of active disease in
80 mouse models and CD patients. Despite this reduction, L cells from inflamed IL-10-deficient mice
81 remained functional regarding GLP-1 secretion. Transcriptional analyses of intestinal epithelial cells
82 indicate altered differentiation correlating with an inflammatory metabolic fingerprint. Reduced GLP-
83 1^{+} cells in ClpP$^{\Delta IEC}$ mice and inhibition of respiration in organoid cultures supports a causative role for
84 metabolism in steering differentiation.

85 **Conclusion** Reduction of GLP-1^{+} cells represents a general feature of ileal and colonic inflammation
86 in mice and human. Given the numerous properties of GLP-1, this reduction likely affects
87 inflammatory processes in the mucosa and disease-related symptoms on multiple levels, and therefore,
88 should be considered a therapeutic target in IBD.

89 **Keywords:** Glucagon-like peptide 1; L cells; Enteroendocrine cells; inflammatory bowel disease

1 Introduction

Enteroendocrine cells (EECs) are renowned for regulating gastrointestinal motility, secretion of digestive fluids, and inducing insulin release *via* peptide hormones. In particular, glucagon-like peptide 1 (GLP-1) has gained enormous attention due to its insulinotropic action and relevance in the treatment of type 2 diabetes and obesity (1). EECs constitute approximately 1% of intestinal epithelial cells (IECs) and are scattered throughout the intestine (2). The intestinal epithelium itself is a key player in maintaining metabolic and immune homeostasis. Ensuring efficient nutrient absorption and at the same time forming a barrier for host defense (3), IECs constitute the body´s most important and dynamic interface to the external environment (4). Stem cells localized at the crypt base expressing leucine-rich repeat-containing G-protein coupled receptor 5 (Lgr5) constantly divide and renew the IEC layer within 3-5 days (5), giving rise to different subtypes of IECs. These subtypes, comprising enterocytes, Paneth cells, goblet cells, tuft cells, M cells, and EECs (6), fulfill specialized functions, with absorptive enterocytes and secretory (mucin-producing) goblet and (antimicrobial peptides-producing) Paneth cells accounting for the largest proportion of IECs.

The regulation of stem cell renewal, proliferation and differentiation is of particular importance under pathological conditions, such as wound healing, tissue regeneration and acute and chronic inflammation as seen in inflammatory bowel diseases (IBD). IBD comprises ulcerative colitis (UC) and Crohn's disease (CD), which are characterized by relapsing inflammation of the colon (UC) or different areas of the gastrointestinal tract but predominantly affecting the terminal ileum (CD). The current paradigm for IBD pathogenesis is a dysregulated interaction between the intestinal microbiota and the mucosal immune system. Consequently, failure of IECs as mediators between these two major factors influencing intestinal inflammation (3) may critically contribute to IBD pathogenesis (7).

Alterations in IEC subpopulations and aberrances of the intestinal stem cell niche have been described in the context of intestinal inflammation. The reduction of secretory goblet cells and Paneth cells (7-9) are the best-studied phenomena in this context. However, upon parasite infection increases in tuft cells,

115 CCK-positive cells, and serotonin (5-HT)-producing enterochromaffin cells are also observed (10-12).
116 Yet, GLP-1-expressing L cells as additional members of the secretory linage of IECs have not been
117 thoroughly characterized under inflammatory conditions.
118 Loss of goblet cells and Paneth cells are early events in intestinal inflammation (9, 13) and have been
119 associated with impaired metabolic fitness of IECs (9, 14). In general, the cellular metabolism plays a
120 pivotal role in regulating intestinal epithelial cell proliferation and differentiation, and mitochondrial
121 function actively determines cellular phenotypes and lineage commitment (9, 15-17). Consistently,
122 there is extensive evidence for altered cellular metabolism, mitochondrial dysfunction, and activation
123 of mitochondrial stress signaling in IBD (15, 18, 19). Moreover, genetic risk loci associated with IBD
124 have been mapped to mitochondrial function-associated genes (15, 20-23) and mitochondrial
125 dysfunction-associated aberrances of the intestinal stem cell niche predict disease recurrence in CD
126 patients (9), suggesting alterations in epithelial cell oxidative metabolism not only as a consequence
127 but causal factor in the development of chronic intestinal inflammation.
128 Even though EECs have been identified as source of the disease-relevant cytokine IL-17C in IBD (24),
129 and autoantibodies against the enteroendocrine protein UbE4A are associated with disease behavior
130 (25), studies investigating the role of EECs in IBD pathogenesis are scarce. Yet, particularly GLP-1
131 producing cells might be of interest in the context of inflammation as these cells actively sense the
132 microbiota and bacterial products, and in addition to its role in glucose metabolism, GLP-1 exerts
133 potent anti-inflammatory effects (26, 27). Highlighting the crosstalk between the immune and
134 endocrine system, the GLP-1 receptor is expressed on multiple immune cell populations, including
135 intestinal intraepithelial lymphocytes (28, 29). In addition, general disease symptoms including
136 reduced appetite, anorexia and altered intestinal motility often accompanying intestinal inflammation,
137 might be linked to GLP-1 signaling (2, 30, 31).
138 As the total number of studies investigating GLP-1^{+} cell numbers and function in the context of
139 intestinal inflammation is limited and results are conflicting (26, 27, 32-34), we quantified numbers of

140 GLP-1 expressing cells in 4 different mouse models of ileal and colonic inflammation (*Tnf*$^{\Delta ARE}$ mice
141 (ileitis), IL-10$^{-/-}$ mice and adoptive T cell-transfer model (colitis) as well as *Citrobacter rodentium*-
142 infection (colitis)). Consistent across all models, a reduction of GLP-1^{+} cells confined to the site of
143 active inflammation is evident, which occurs early in the course of inflammation. The remaining GLP-
144 1-expressing L cells in IL-10$^{-/-}$ mice are functional in terms of hormone secretion. Importantly, analysis
145 of a recently published data set from single-cell RNA sequencing of mucosal biopsies from CD patients
146 (35), confirmed the human relevance of these findings. In parallel to EEC loss, colonic IECs of
147 inflamed IL-10$^{-/-}$ mice display a metabolic fingerprint that has been associated with reduced
148 differentiation into other cell types of the secretory lineage (goblet cells, Paneth cells). Remarkably,
149 compromised mitochondrial function in ClpP$^{\Delta IEC}$ mice, as well as inhibition of mitochondrial
150 respiration using oligomycin in murine and human organoid cultures was sufficient to reduce EEC
151 marker gene expression, indicating a causative role for metabolism in steering differentiation into this
152 IEC subtype.

153 **2 Results and discussion**

154 **2.1 GLP-1 positive cells are consistently reduced under inflammatory conditions**

155 To comprehensively characterize the impact of intestinal inflammation on the number of GLP-1-
156 expressing L cells in the epithelium, ileal and colonic tissue sections from different mouse models of
157 intestinal inflammation were immunohistochemically stained (**Figure 1A**). Cells positive for GLP-1
158 were quantified as positive cells over the total epithelial layer (mm^2), to minimize confounders due to
159 architectural changes of the intestinal tissue caused by inflammatory processes such as immune cell
160 infiltration. At least 3 non-consecutive, well-oriented tissue sections per mouse were used for
161 quantification. Group sizes were ≥ 5 in all cases. In accordance with 3R principles, tissue samples
162 analyzed were obtained from our tissue biobank and originated from previous studies (9, 36-38). Mouse
163 models investigated comprise commonly used models of IBD, (I) the *Tnf*$^{\Delta ARE}$ mouse model of ileitis
164 and (II) IL-10 deficient mice as model of colitis; (III) an adoptive T cell transfer model of colitis, Rag2^{-}
165 $^{/-}$ mice reconstituted with CD4^{+} CD25^{-} T cells; and (IV) an infection model using *Citrobacter*
166 *rodentium*. In *Tnf*$^{\Delta ARE}$ mice, CD-like tissue inflammation develops gradually and microbiota-dependent
167 due to loss of translational control of the pro-inflammatory cytokine tumor necrosis factor (Tnf) caused
168 by a deletion of AU-rich (adenosin-uracil) elements (ARE) in the *Tnf* gene/ mRNA, resulting in Tnf
169 overexpression (39). Similarly, mice lacking the anti-inflammatory cytokine interleukin 10 (IL-10$^{-/-}$
170 mice) spontaneously develop colitis after weaning whereby onset and severity of inflammation are
171 dependent on the microbiota and the genetic background of mice (40), with the 129/SvEv mouse line
172 being more susceptible than C57BL/6 mice. In the following, "IL-10$^{-/-}$ mice" refers to inflamed
173 129/SvEv IL-10 deficient mice unless otherwise stated. The T cell transfer model of colitis is the most
174 widely used model of IBD to dissect the contribution of T cells to immunopathology in chronic colitis
175 (41). Notably, the expansion of enterochromaffin cells, a cell type closely related to EECs, is dependent
176 on T cell presence during helminth infection (10), indicating a direct effect of immune cells on
177 epithelial cell composition. In contrast to the models of chronic inflammation, infection with *C.*

178 *rodentium* causes transient colonic inflammation and hyperplasia and serves as a model to study host-
179 pathogen interaction in the context of IBD and to study molecular mechanisms of human
180 gastrointestinal infections with pathogenic *Escherichia coli* strains (42).
181 In a first approach, we compared moderately inflamed mice (histopathological score (HS) 2-4) of the
182 different models to wild type (Wt) littermates or non-reconstituted/ non-infected mice, respectively
183 (**Figure 1B-E**). Consistently throughout all models investigated, numbers of GLP-1^{+} cells were
184 reduced under inflammatory conditions (**Figure 1B-E**). These changes were observed at the site of
185 active disease, namely the ileum in *Tnf*$^{\Delta ARE}$ mice (**Figure 1B**) and the colon in IL-10$^{-/-}$ mice, Rag2$^{-/-}$
186 mice adoptively transferred with colitogenic CD4^{+} CD25^{-} T cells, and C57BL/6 mice infected with *C.*
187 *rodentium* (**Figure 1C-E**). Of note, during infection with *C. rodentium*, loss of GLP-1^{+} cells was
188 transient and paralleled tissue aberration in the progressive and regressive phases of infection, with
189 protein expression returning to basal numbers after bacterial clearance (day 32) (**Figure 1E**). Reflecting
190 cell numbers, we observed diminished expression levels of *Gcg* (*glucagon*, translated *i.a.* into GLP-1
191 in the intestine) at the site of active disease in *Tnf*$^{\Delta ARE}$ mice and IL-10$^{-/-}$ mice but not unaffected tissue
192 regions (proximal colon and distal ileum, respectively) (**Figure 1F,G**), indicating a local and acute
193 effect of inflammatory processes on intestinal epithelial cell composition. Loss of IL-10 receptor has
194 been shown to disrupt IEC proliferation and skew differentiation towards the goblet cell fate,
195 implicating a role for IL-10 signaling in IEC lineage decisions (43). Yet, corroborating an
196 inflammation-mediated over a genetic effect, we did not find any reduction in GLP-1^{+} (**Figure 1H,I**)
197 in non-inflamed IL-10$^{-/-}$ mice on C57BL/6 background or Rag2$^{-/-}$ mice reconstituted with regulatory
198 CD4^{+} CD25^{+} T cells, thus not developing colitis. Notably, the reconstitution of Rag2$^{-/-}$ mice with
199 regulatory T cells did not exert any effect on GLP-1^{+} cell numbers (**Figure 1H**), suggesting lack of T
200 cell-mediated regulation under homeostatic conditions.
201 For characterizing the effect of inflammation on EECs numbers in detail, we took advantage of the
202 heterogeneity in the grade of CD-like inflammation in *Tnf*$^{\Delta ARE}$ mice and of colitis in IL-10$^{-/-}$ mice. In

203 independent, additional cohorts, we quantified numbers of GLP-1^{+} across a broad range of
204 histopathological scores. Numbers of cells positive for GLP-1 inversely correlated with the grade of
205 inflammation in the ileum of *Tnf*$^{\Delta ARE}$ mice (**Figure 1J**) and in the colon of IL-10$^{-/-}$ mice (**Figure 1K**).
206 Comparing tissues from non-inflamed (HS <2) *Tnf*$^{\Delta ARE}$ mice and Wt C57BL/6 littermates as well as
207 IL-10$^{-/-}$ mice and Wt 129/SvEv controls, we observed no differences in the total numbers of GLP-1^{+}
208 (**Figure 1B,C,J,K**). Thus, loss of EECs parallels the progression towards an inflammatory tissue
209 environment.
210 To confirm the human relevance of our findings, we used a recently published single-cell RNA
211 sequencing data set from mucosal biopsies comprising healthy controls, as well as inflamed and non-
212 inflamed tissues from CD patients (35). A total of 154,136 epithelial cells derived from terminal ileum
213 (**Figure 1L**) and 97,788 colonic epithelial cells (**Figure 1M**), respectively, were clustered into
214 subgroups and EECs were analyzed for *GCG* expression. In both the terminal ileum and colon, the
215 percentage of epithelial cells expressing *GCG* dropped in the inflamed mucosa and was already altered
216 in tissues that did not appear inflamed by endoscopic examination compared to healthy controls. This
217 is in line with the data from IL-10$^{-/-}$ and *Tnf*$^{\Delta ARE}$ mice and suggests either the presence of low-grade
218 inflammation or a persistent shift in epithelial subtype composition even in the absence of acute
219 inflammation.
220 Notably, also the proportion of *GCG* expressing cells among EECs was reduced, indicating GLP-1-
221 producing L cells to be particularly affected by inflammation (**Figure 1L,M**). Technical advances have
222 overturned the one cell-one hormone dogma for EECs (44, 45), and thus, L cells co-express GLP-1
223 with different hormones depending on their location. Peptide YY (PYY) is one of these hormones and
224 shows an expression pattern in the mammalian gastrointestinal tract similar to that of GLP-1 (46).
225 Corroborating the hypothesis of L cell susceptibility to inflammation, the proportion of *PYY*-expressing
226 EECs also decreased under inflammatory conditions in patients, in both the terminal ileum (**Figure**
227 **1N**) and colon (**Figure 1O**). Mirroring these results, also in the murine ileitis model (*Tnf*$^{\Delta ARE}$) and

228 colitis model (IL-10$^{-/-}$) *Pyy* expression was reduced in inflammation-affected intestinal tissues (**Figure**
229 **1N,O**).
230
231 **2.2 Inflammatory conditions impair epithelial differentiation into EECs**
232 The intestinal epithelium constantly renews, and a tight balance between cell proliferation,
233 differentiation, and apoptosis/ cell shedding is required to sustain homeostasis. Alterations in intestinal
234 epithelial cell differentiation, subtype composition, and cell functions are part of the pathology of
235 intestinal inflammation (15, 47).
236 Thus, we performed a transcriptional analysis of isolated intestinal epithelial cells from moderately
237 inflamed IL-10-deficient mice and Wt littermates. Expression of transcription factors involved in
238 epithelial differentiation and marker genes of epithelial subpopulations indicated reduced terminal
239 differentiation of epithelial cells under inflammatory conditions (**Figure 2A,B**). This is consistent with
240 crypt hyperplasia and expansion of the transit-amplifying zone, both histologic hallmarks of
241 inflammation. EECs arise from the secretory linage, which also comprises antimicrobial peptide-
242 producing Paneth cells (in the small intestine), Paneth-like cells (in the large intestine), mucin-
243 producing goblet cells, serotonin-producing enterochromaffin cells, and tuft cells involved in
244 chemosensing (**Figure 2B**). Secretory cells are particularly affected by inflammatory processes. For
245 example, we found reduced numbers and functionality of Paneth cells in parallel to aberrations of the
246 stem cell niche in CD patients and *Tnf*$^{\Delta ARE}$ mice (9, 39). Furthermore, goblet cell-loss is a common
247 feature of *C. rodentium*-triggered colonic inflammation (42) as well as genetically-driven colitis
248 observed in IL-10$^{-/-}$ mice (48). Accordingly, we found an mRNA expression pattern indicating
249 diminished presence of secretory precursor cells and reduced marker gene expression for all secretory
250 cells except enterochromaffin cells (**Figure 2A,B**). Immunohistochemical staining and quantification
251 of positive cells confirmed decreased numbers of Doublecortin-like kinase protein 1 (Dclk1)$^{+}$ tuft cells
252 but stable numbers of serotonin containing (5-HT^{+}) enterochromaffin cell under inflammatory

253 conditions in IL-10$^{-/-}$ mice (**Figure 2C,D**), suggesting mechanisms specifically sustaining this cell
254 population under inflammatory conditions.
255 Of note, a hierarchical cascade of transcription factors acts in a combinatorial fashion to steer
256 differentiation of Neurogenin 3 (Neurog3)-expressing progenitor cells into the diverse EEC subtypes
257 (46). Neurog3 itself is required to restrict secretory progenitors to the endocrine lineage (49) and was
258 increased in intestinal epithelial cells from inflamed IL-10$^{-/-}$ mice (**Figure 2A,B**). An early event in
259 EEC differentiation is whether the cell commits to the enterochromaffin or peptidergic lineage. This
260 decision is regulated by the transcription factor Regulatory factor 6 (Rfx6), which promotes expression
261 of peptidergic hormones while repressing 5-HT synthesis *via* LIM homeobox transcription factor alpha
262 (Lmx1a) (50). Accordingly, Rfx6 acts upstream of late acting transcription factors Aristaless-related
263 homeobox (Arx), Paired box gene (Pax) 6 and Insulin gene enhancer protein (Isl) 1, regulating
264 enterohormone gene transcription and as such, controlling terminal differentiation of enteroendocrine
265 cell subtypes (46). Consequently, loss of Rfx6 in the epithelium causes accumulation of Neurog3-
266 positive enteroendocrine progenitors and expansion of 5-HT-positive enterochromaffin cells,
267 accompanied by impaired differentiation of peptide-producing EECs (50). Although this resembles the
268 situation observed under inflammatory conditions, expression of *Arx*, *Pax6*, *Isl1* and *Lmx1a* was
269 increased under inflammatory conditions in intestinal epithelial cells from IL-10$^{-/-}$ mice (**Figure
270 2A,B**)., arguing against Rfx6 as key driver of skewed differentiation.
271 Employing the same single-cell RNA sequencing data set (35) as before, a similar pattern was observed
272 in CD patients. There was a reduction in colonic epithelial cells expressing the mature colonocyte
273 marker *CA1* (*Carbonic anhydrase 1*) under inflammation (**Figure 2E**). Concomitantly, the proportion
274 of EECs expressing the enterochromaffin cell marker *TPH1* (*Tryptophan hydroxylase1*) and the
275 proportion of epithelial cells expressing *NEUROG3* increased in CD patients independent of the
276 inflammatory status (**Figure 2E**). Further reflecting the gene expression pattern of inflamed IL-10$^{-/-}$
277 mice, the proportion of EECs expressing *ARX*, *PAX6*, *Isl1, LMX1A* and *RFX6* were increased in CD

278 patients (**Figure 2F**). Interestingly, a tight bi-directional interaction of L cells and enterochromaffin
279 cells has been described, with L cells expressing serotonin receptor 4 (51) and enterochromaffin cells
280 expressing GLP-1 receptor (52). Moreover, endocrine cell differentiation is facilitated through
281 paracrine GLP-1 and serotonin-mediated signaling involving Neurog3 (53).

282 **2.3 Remaining colonic L cells are functional**

283 The transcription factors *Pax6* and *Isl1* directly bind consensus sequences on the *Gcg* promoter,
284 indicating a sustained expression of *Gcg* in the reduced number of GLP-1^{+} cells in the epithelium.
285 Following translation, proglucagon encoded by *Gcg* is cleaved into active GLP-1 by prohormone
286 convertase (PC) 1/3 in EECs. Subsequent to secretion, active GLP-1 is rapidly cleaved and inactivated
287 by dipeptidyl peptidase-4 (DPP4) in target tissues, resulting in a half-life of only 2 minutes (54, 55)
288 (**Figure 2G, scheme**). In accordance with the hypothesis that remaining EECs sustain GLP-1
289 expression, *Pcsk1* (encoding PC1/3) expression remained unaltered under inflammation in IL-10$^{-/-}$
290 mice, whereas expression of *Dpp4* strongly decreased specifically at the site of inflammation (proximal
291 colonic tissue) (**Figure 2G**), suggesting compensatory mechanisms to maintain GLP-1 signaling.
292 Corroborating these results, we found reduced but substantial amounts of active GLP-1 in primary
293 colonic crypts derived from IL-10$^{-/-}$ mice (**Figure 2H**). Furthermore, L cells remained functional as
294 primary colonic organoids derived from IL-10$^{-/-}$ mice showed a secretory response towards stimulation
295 with the bile acid deoxycholic acid (DCA) that did not significantly differ from that of Wt organoids
296 (3.3 ± 0.36 *vs* 2.1 ± 0.28 fold increase), despite overall reduced secretion of GLP-1 per living cell
297 (**Figure 2I**). Likewise indicating reduced but functional L cells, the average expression of *GCG* within
298 colonic *GCG*$^{+}$ cells remained unaltered in the single-cell RNA sequencing data set (35) in CD patients
299 compared to healthy controls (**Figure 2J**).

300 **2.4 Inflammatory cytokines and microbial structures affect *Gcg* expression**

301 To investigate a potential contribution of pro-inflammatory cytokines and microbial structures to the
302 inflammatory environment fostering L cell loss, we employed intestinal organoids derived from Wt

303 mice. First, we tested whether microbial structures including bacterial muramyl dipeptide (MDP) and
304 lipopolysaccharide (LPS) or the pro-inflammatory cytokines interferon γ (IFN) and TNF would induce
305 GLP-1 secretion (**Figure 3A**). MDP is a substrate of PEPT1, known to mediate di/tripeptide-induced
306 GLP-1 secretion in L cells and can be sensed intracellularly by nucleotide-binding oligomerization
307 domain (NOD)-like receptors that belong to the innate immune system (56). SNPs in both *Pept1* and
308 *Nod2* are known risk factors for IBD (57, 58). Yet, neither MDP nor treatment with a mixture of
309 IFN/TNF led to a detectable secretion of GLP-1 despite responsiveness of organoids towards the bile
310 acid deoxycholic acid (DCA) (**Figure 3B**). In contrast, LPS acted as a weak GLP-1 secretagogue, in
311 accordance with literature proposing TLR4-dependent GLP-1 secretion upon LPS exposure by L cells
312 as pathogen sensing mechanism during intestinal injury (59). A mixture of forskolin/3-isobutyl-1-
313 methylxanthine (F/I) served as a control for maximal hormone output (**Figure 3B**).
314 In a second approach, organoids were stimulated with low concentrations of TNF/IFN and LPS for 48h
315 to determine the effect on epithelial differentiation. The chosen concentrations did not impair organoid
316 survival or growth after 48h (**Figure 3C,D**), but robustly induced Interferon gamma-induced protein
317 10 (IP-10) in cell lysates and supernatants after 8h (**Figure 3E,F**), indicating reactivity towards
318 stimulation. Treatment for 48h with TNF/IFN resulted in diminished expression of *Gcg* and *Mucin 2*
319 (*Muc2*), a marker for goblet cells, recapitulating *in vivo* inflammatory conditions (**Figure 3G**). In
320 contrast, LPS treatment increased *Gcg* and *Muc2* expression (**Figure 3H**), which supports the
321 hypothesis that persistent activation of L cells stimulates L cell differentiation in a paracrine manner
322 (60) and data showing LPS-mediated upregulation of mucin expression and secretion in goblet cells
323 (61).

324 **2.5 Inflammation-associated impairment of mitochondrial metabolism is associated with**
325 **reduced enteroendocrine cell markers**

326 A potential mechanism by which TNF/IFN and inflammation might affect L cell numbers is by
327 affecting cellular metabolism and particularly mitochondrial function, including oxidative

328 phosphorylation (OXPHOS) (15, 62, 63). Previously, we established a link between impaired
329 mitochondrial function and altered epithelial cell differentiation in the context of intestinal
330 inflammation (9, 14, 64, 65). In particular, we found an inflammation-related metabolic fingerprint in
331 ileal epithelial cells comprising a shift from OXPHOS to glycolysis and overall reduced cellular ATP
332 level in *Tnf*$^{\Delta ARE}$ mice. These metabolic changes were paralleled by induction of mitochondrial stress
333 signaling pathways and aberrances of the intestinal stem cell niche, including loss of Paneth cells (9).
334 On the basis of these results we screened genes indicative for different inflammation-relevant cellular
335 metabolic pathways and metabolic genes known to affect the intestinal stem cell niche (16, 65) in
336 isolated intestinal epithelial cells from moderately inflamed IL-10-deficient mice and Wt littermates
337 (**Figure 4A**). Reflecting previous observations, transcriptional analysis indicated holistic metabolic
338 changes in colitis, including reduced mitochondrial metabolism, enhanced glycolysis and activation of
339 autophagy (66). Genes involved in the dynamic metabolic adaptions required for maintaining
340 homeostasis of the ISC niche (including *Pdk4, Sgk1, Hmgcs2* and *Mtor*) were consistently down-
341 regulated (**Figure 4A,B**). Concomitantly, cellular ATP levels were reduced and expression of *Trib3*, a
342 marker for activation of the mitochondrial unfolded protein response (MT-UPR), a signaling pathway
343 related to disturbances of mitochondrial function, was enhanced (**Figure 4C,D**). Highlighting the
344 strong link between inflammation-related epithelial metabolism and *Gcg* expression, mRNA levels of
345 *Hk2* and *Ddit4*, genes involved in glycolysis and suppressing mammalian target of rapamycin (mTOR)
346 activity (67, 68), negatively correlated with *Gcg* expression, while a positive correlation was observed
347 for *Pck1* and *Hmgcs2*, genes involved in gluconeogenesis and ketogenesis, respectively (**Figure 4E**).
348 Importantly, these finding were reflected by the single-cell RNA sequencing data set derived from
349 human mucosal biopsies. The frequency of colonic epithelial cells expressing marker genes for
350 mitochondrial stress signaling (*TRIB3*, *ATF5*) and reduced cellular ATP levels (*PRKAA1* encoding the
351 catalytic subunit of AMPK) was increased in tissues from inflamed CD patients (**Figure 4F**).
352 Concomitantly, the proportion of colonic epithelial cells expressing metabolism-associated genes *HK2*

353 and *DDIT4* was elevated under inflammatory conditions, while the proportion of cells expressing
354 *PCK1* and *HMGCS2* decreased (**Figure 4G**). In line with previous results, most changes in cellular
355 expressions were also visible in epithelial cells derived from biopsies of CD patients that were
356 considered non-inflamed, again pointing toward cellular metabolic alterations preceding overt tissue
357 pathology or persisting in the absence of the same. In summary, these data indicate that, consistent
358 with ileal inflammation (9), colonic inflammatory processes are also associated with mitochondrial
359 stress and are paralleled by reprogramming of intestinal cellular metabolism, dampening OXPHOS,
360 and fostering glycolysis. This metabolic fingerprint accompanies the decline in GLP-1 positive cell
361 numbers.

362 **2.6 Mitochondrial impairment causes reduction of enteroendocrine cells**

363 Intriguingly, deletion of the mitochondrial chaperone Hsp60 in murine colonocytes, triggering
364 mitochondrial dysfunction and stress signaling, resembles the metabolic fingerprint of inflammation
365 including up-regulation of *Hk2* and *Ddit4*, as well as down-regulation of *Pck1* and *Hmgcs2* (65).
366 Elegantly demonstrating the causative contribution of metabolic disturbances to altered epithelial
367 differentiation, this genetic model of primary mitochondrial dysfunction also shows a reduction in
368 differentiated cells, including EECs, enterocytes, and tuft cells (but not enterochromaffin cells), as
369 shown by single-cell RNA sequencing (65). To further establish mitochondrial impairment as a key
370 driver of skewed epithelial differentiation processes, we used a mouse model with an epithelial-specific
371 knockout of caseinolytic mitochondrial matrix peptidase ($ClpP^{\Delta IEC}$). ClpP contributes to mitochondrial
372 proteostasis and knockout of ClpP triggers induction of Trib3 (69), Atf5 (70) and activation of AMPK
373 (71). Tissue-specific ClpP deficiency in liver and skeletal muscle causes mitochondrial dysfunction
374 including a decrease in mitochondrial respiratory supercomplexes (70). In contrast to Hsp60, whose
375 non-inducible IEC-specific knockout (using *Villin1*Cre transgenic mice) is embryonic lethal (64),
376 $ClpP^{\Delta IEC}$ mice are viable and exhibit normal growth and body weight development on a standard chow
377 diet (data not shown), indicating less severe mitochondrial impairment. Epithelial loss of ClpP was

378 confirmed by qPCR analysis of *ClpP* mRNA in isolated IECs (**Figure 5A**). Morphological features of
379 the small intestine and colon including intestinal length, number of crypts (quantifications not shown),
380 and crypt/villus length were similar to control *ClpP*$^{flox/flox}$ littermates at the age of one year (**Figure**
381 **5B,C**). On the cellular level, proliferation (quantified by number of Ki67-positive cells per crypt)
382 remained unchanged as well as the number of mucin-producing goblet cells (identified by PAS/AB
383 staining) (**Figure 5C**). However, plasma concentration of citrulline, synthesized in the small intestinal
384 epithelium as part of the urea cycle and serving as a functional readout of IEC mitochondrial function,
385 was decreased in ClpP$^{\Delta IEC}$ mice, in line with previous results from Hsp60$^{\Delta IEC}$ mice (64) (**Figure 5D**).
386 Additionally, Paneth cells from ClpP$^{\Delta IEC}$ mice contained fewer granules positive for the antimicrobial
387 peptide lysozyme (Lyz^{+}) (**Figure 5E,F**), despite overall Paneth cell abundance remaining unchanged
388 (data not shown). Disturbances of AMP-packaging into granules and alterations in the granule
389 exocytosis pathway manifest as disorganized and reduced numbers of cytoplasmic granules as well as
390 a diffuse cytoplasmic lysozyme expression (8) (**Figure 5F, scheme**). Therefore, morphology of Lyz^{+}
391 secretory granules is used as a functional marker for Paneth cell phenotype classification, and both
392 inflammation and epithelial mitochondrial dysfunction have previously been shown to correlated with
393 reduced Paneth cell granularity (8, 9). Importantly, numbers of GLP-1^{+} cells were diminished in the
394 ileum and proximal colon in ClpP$^{\Delta IEC}$ mice (**Figure 5G**), indicating that mild mitochondrial
395 dysfunction in the absence of tissue aberration or overt inflammation is sufficient to compromise
396 Paneth cell function and reduce EEC differentiation.
397 To further validate that disturbances of mitochondrial metabolism skew epithelial differentiation, we
398 used the OXPHOS inhibitor oligomycin *ex vivo* in intestinal organoids. Murine intestinal Wt organoids
399 (**Figure 5H**) and human intestinal organoids (**Figure 5I**) were treated with sub-lethal doses of
400 oligomycin for 6h and were subsequently allowed to recover for 18h. Blockade of OXPHOS induced
401 mitochondrial stress signaling (MT-UPR) as evidenced by *Trib3*/ *TRIB3* upregulation and led to a
402 reduction of the enteroendocrine marker gene *Chga*/ *CHGA*, in both murine and human organoids

403 (**Figure 5H-I**). In summary, these data support the notion that impaired mitochondrial function in
404 epithelial cells, as observed under inflammatory conditions, might be the driving force of reduced GLP-
405 1^+ cell numbers.

406 **3 Conclusion**

407 While the mechanisms underlying hormone secretion from L cells and their functions in the context of
408 digestion and metabolism are well studied, their role in the pathogenesis of intestinal inflammation is
409 virtually unknown.

410 Quantifying GLP-1^+ cells in four mouse models of ileitis and colitis and characterizing two
411 independent cohorts of each *Tnf*$^{\Delta ARE}$ mice and IL-$10^{-/-}$ mice, we found a consistent reduction in GLP-1
412 expressing cells confined to the site of active disease and correlating to the degree of inflammation.
413 Importantly, we confirmed the reduced expression of the GLP-1-encoding gene *GCG* in a publicly
414 available single-cell RNA sequencing data set of ileal and colonic mucosal biopsies derived from
415 healthy controls as well as inflamed and non-inflamed tissues from CD patients (35). Hence, the loss
416 of GLP-1^+ cells appears to be a general feature of both small and large intestinal inflammation. One
417 major goal of this work was to give a comprehensive overview of different mouse models of intestinal
418 inflammation and therefore, most tissue samples used were generated in the context of previous studies.
419 This explains the lack of GLP-1 measurements in plasma, a clear limitation that has to be overcome in
420 subsequent studies. However, previous data do not indicate a reduced glucose tolerance in IL-10
421 deficient mice (66). This could be attributed to location-specific functions that have been proposed for
422 GLP-1, with ileal GLP-1 stimulating insulin release in response to nutrients (72) and colonic GLP-1
423 exerting rather local effects, *i.e.*, slowing gastrointestinal transit time (73).

424 Regarding IBD patients, available data for plasma GLP-1 levels remain inconsistent (27). This may be
425 due to methodological differences (74), but also biological challenges, including the heterogeneity of
426 IBD pathologies and the fact that only about 10–15% of secreted GLP-1 reaches the systemic

427 circulation in its active form (54, 55). Moreover, total changes in hormone secretion depend on the
428 severity of inflammation and the extent of tissue affected and therefore, might be too minor to be
429 recovered systemically. Beyond their classical endocrine function, being secreted into the bloodstream
430 to act on receptor-expressing cells in distant target tissues, EEC-derived hormones also signal to
431 neighboring cells in the epithelial layer and the lamina propria. Thus, even if systemic changes in GLP-
432 1 levels might not be readily detectable, altered paracrine signaling of GLP-1 could have profound
433 effects on enterochromaffin cells (as mentioned above) (51-53), intraepithelial lymphocytes (29) and
434 afferent neurons, in turn impacting intestinal motility, mucosal immune responses and feeding behavior
435 under inflammatory conditions (75).
436 In particular, a subset of EECs termed "neuropod cells", capable of forming synapses with neurons
437 innervating the small intestine and colon, has gained increasing attention (75). Acting as sensory
438 epithelial cell, neuropod cells form a neuroepithelial circuit that transduces signals between gut and
439 brain (76). Terminal fibers of the vagus nerve, among others, express receptors for multiple EEC
440 hormones and also enterochromaffin cell-derived serotonin acts on intestinal neurons (77). For
441 instance, the effects of GLP-1 on food intake and glucose homeostasis are, at least in part, neurally
442 mediated (78, 79), and co-release of GLP-1 and ATP from neuropod cells has been shown to elicit a
443 vagal response (80). These neuroepithelial signals are thought to participate in sensing of nutritional
444 value and the regulation of satiety, reward of food and peristaltic activity (75).
445 Furthermore, EECs are an integral part of the intestinal epithelial barrier, interacting with the
446 microbiome as well as the mucosal immune system. Sensing the luminal and lamina propria
447 environment, EECs not only react to bacterial structures like LPS through pattern recognition receptors
448 (72, 81, 82), and bacterial metabolites such as SCFA and indole (83), but also express TNF receptor 1
449 (84). In addition to GLP-1 release, exposure to flagellin or lipopolysaccharide (85, 86) also results in
450 expression of pro-inflammatory cytokines and evokes a gene response indicating EECs to participate
451 in innate immune responses to commensals and pathogens (85). Highlighting the role of GLP-1 in

452 regulating immune responses, gastrointestinal intraepithelial lymphocytes express the GLP-1 receptor
453 (29), establishing a local enteroendocrine L cell-intraepithelial lymphocyte axis. GLP-1R signaling in
454 intraepithelial lymphocytes selectively restrains local and systemic T cell-induced inflammation by
455 suppression of effector functions, and modulates microbiota composition (87). These properties are of
456 particular relevance in the context of IBD, where dysbiosis and dysregulated immune responses
457 towards commensal constituents of the microbiota are thought to play a critical role in pathogenesis
458 (14).
459 Hormone expression patterns of L cells differ considerably depending on their location in the intestine
460 (88-90) and GLP-1 is co-expressed with other hormones including GLP-2, PYY, glucose-dependent
461 insulinotropic polypeptide GIP, cholecystokinin (CCK) and secretin. Thus, the reduction of GLP-1
462 expressing cells under inflammatory conditions in the intestine should also profoundly affect signaling
463 of additional gut hormones. Indeed, next to *GCG*, we also found a reduction in *PYY* expressing cells,
464 which is in agreement with a study using colonic epithelial cells from treatment-naïve adult CD patients
465 (47). With regard to mucosal homeostasis, GLP-2, posttranslationally processed from proglucagon like
466 GLP-1 and secreted in equimolar amounts (91), is of particular interest. GLP-2 is an epithelial growth
467 factor implicated in tissue healing following injury, improving barrier function and restoring epithelial
468 homeostasis. Furthermore, GLP-2 possesses anti-inflammatory properties and sustains Paneth cell
469 function (92). Consequently, it has been shown to ameliorate experimental colitis in several animal
470 models (93-96) and a GLP-2 analog was proven effective in the treatment of active moderate to severe
471 CD (97).
472 Importantly, we link the loss of GLP-1^{+} cells to an inflammation-related epithelial metabolic signature
473 that was previously associated with impaired Paneth cell and goblet cell differentiation (9, 14) and that
474 is reflected in colonic epithelial cells of CD patients. In accordance with the pivotal role of
475 mitochondria in steering differentiation processes by balancing OXPHOS and glycolysis,

476 compromised mitochondrial function in ClpP$^{\Delta IEC}$ mice, as well as *ex vivo* inhibition of OXPHOS in
477 organoid cultures, was sufficient to impair EEC development.
478 This is in line with previous data (9, 98) and points toward compromised mitochondrial function as
479 underlying cause of altered epithelial cell composition during the onset of inflammatory processes.
480 Underlining the translatability of findings to the human disease condition, a downregulation of the
481 ketogenesis pathway, as expected by a drop in *HMGCS2* expression, has been described for
482 colonocytes of CD patients (35) and in line, reduced levels of the ketone body β-hydroxybutyrate were
483 observed in the colonic mucosa of IBD patients which correlated with IBD activity index (99). Of note,
484 a similar pattern of *HK2* expression to that we found in the single-cell RNA sequencing data set of CD
485 patients (lowest in healthy controls and gradual increase from non-inflamed to inflamed tissue samples
486 from IBD patients) has recently been reported in another cohort of IBD patients (100).
487 Remarkably, analysis of the single-cell RNA sequencing data set CD patients revealed metabolic
488 changes and signs of mitochondrial stress signaling as well as changes in epithelial subtype
489 composition even in mucosal tissues that were considered non-inflamed by endoscopy. Considering
490 the chronic remittent pathology of CD with phases of remission and flares of inflammation, these
491 cellular metabolic changes might render the mucosa susceptible for additional inflammatory triggers.
492 Consequently, improving metabolic fitness and metabolic reprogramming have been identified as new
493 therapeutic targets combating IBD by restoring functionality of IEC subtypes and enforcement of the
494 epithelial regenerative capacity (14). Although so far rather neglected as player in intestinal
495 inflammation, EECs might also profit from such metabolic interventions.
496 Recently, the influence of GLP-1 receptor agonists on the disease course of CD and UC patients with
497 concomitant type 2 diabetes was investigated in a large-scale cohort study. The results suggest a
498 potential therapeutic advantage of GLP-1 receptor agonists in managing IBD, by reducing
499 hospitalizations, surgeries, and mortality (101). These beneficial outcomes underline the need for more
500 research to scrutinize the role of GLP-1 in the pathogenesis of intestinal inflammation. However, given

501 the numerous properties of GLP-1, it is likely that it affects inflammatory processes in the mucosa and
502 disease-related symptoms on multiple levels (**Figure 6**). Thus, EECs and GLP-1-based therapies could
503 represent an independent, promising strategy for intestinal inflammatory diseases.
504

4 Figures + Legends

4.1 Figure 1: GLP-1$^+$ cells are reduced in the murine and human intestinal mucosa under inflammatory conditions

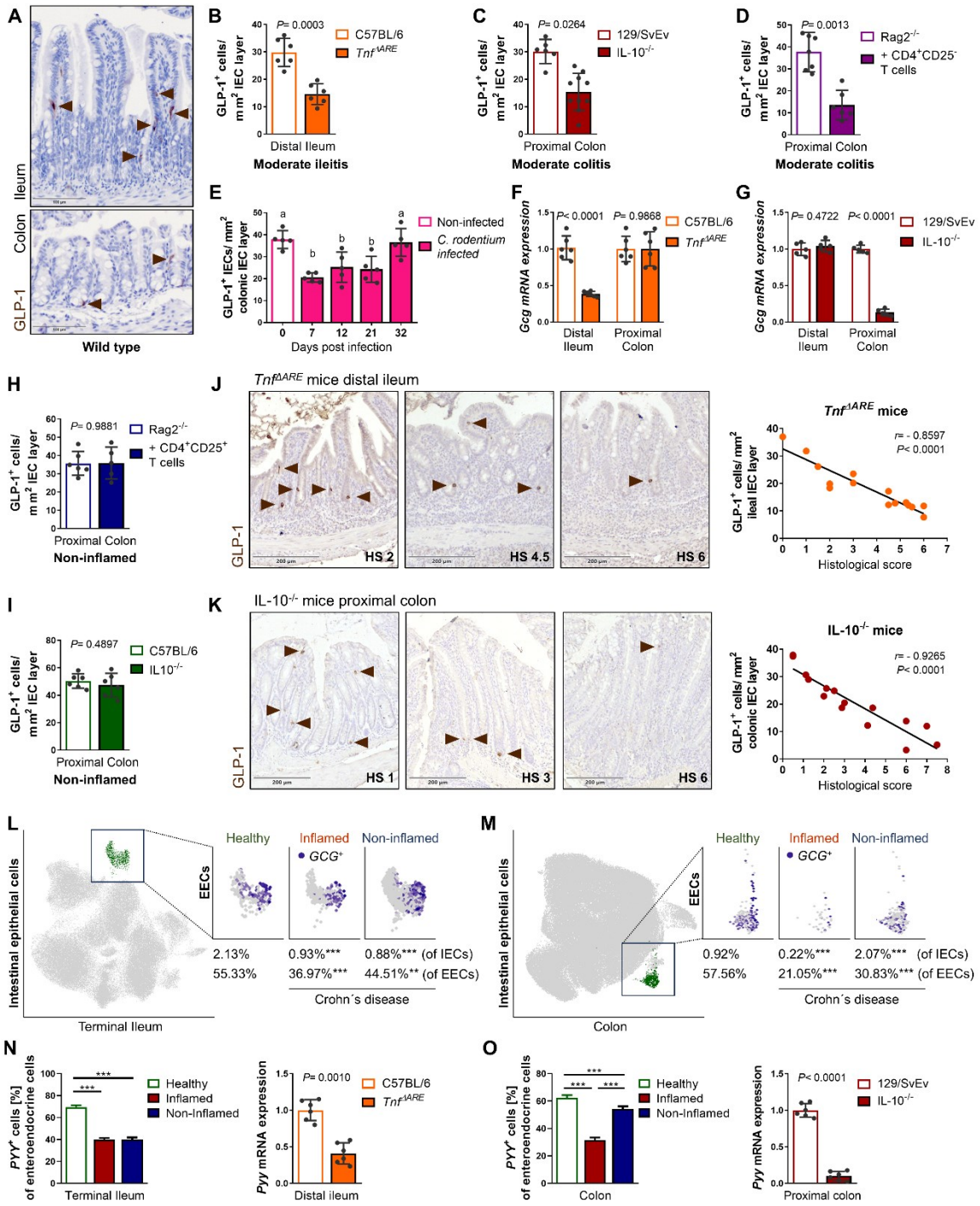

509 (**A**) Representative pictures of ileal and colonic tissue sections from wild type mice
510 immunohistochemically (IHC) stained for GLP-1. Arrows indicate cells positive for GLP1. (**B-D**)
511 Quantification of GLP-1-positive cells (**B**) in ileal tissue sections of moderately inflamed (histological
512 score (HS) 2-4) *Tnf*$^{\Delta ARE}$ mice, (**C**) in colonic tissue sections of moderately inflamed IL-10$^{-/-}$ mice, (**D**)
513 in colonic tissue sections of moderately inflamed Rag2$^{-/-}$ mice adoptively transferred with colitogenic
514 CD4^{+} CD25^{-} T cells, and respective controls. (**E**) Quantification of GLP-1-positive cells in colonic
515 tissue sections of mice infected with *Citrobacter (C.) rodentium* prior to and at different time points
516 post infection. (**F, G**) qRT-PCR analysis for *Gcg* (encoding GLP-1) of ileal and colonic tissue from
517 (**F**) *Tnf*$^{\Delta ARE}$ mice and (**G**) from IL-10$^{-/-}$ mice including respective controls. Expression levels are
518 normalized to controls and tissue of origin. (**H, I**) Quantification of GLP-1-positive cells in colonic
519 tissue sections (**H**) of non-inflamed Rag2$^{-/-}$ mice adoptively transferred with regulatory CD4^{+} CD25^{+}
520 T cells and (**I**) of non-inflamed IL-10$^{-/-}$ mice on C57BL/6 background and respective controls. (**J, K**)
521 Representative GLP-1 IHC stainings for the HS indicated (left) and correlation analysis (Pearson) of
522 the number of GLP-1-positive cells and HS for (**J**) ileal tissue from *Tnf*$^{\Delta ARE}$ mice and (**K**) colonic tissue
523 from IL-10$^{-/-}$ mice. (**L**, **M**) Uniform manifold approximation and projection (UMAP) visualization of
524 scRNA-sequencing of intestinal epithelial cells from the terminal ileum (**L**) and colon (**M**) from
525 Crohn´s disease patients (35). The subgroup of enteroendocrine cells is highlighted in green (left) and
526 *GCG*-expressing enteroendocrine cells are shown in purple in healthy, inflamed and non-inflamed
527 conditions (right). The sample size for healthy/ inflamed/ non-inflamed is 11/ 14/ 45 for (**L**) and 32/ 5/
528 18 for (**M**), respectively. Chi-square test and Fisher´s exact test, asterisks indicate differences compared
529 to healthy controls, *P<0.05, **P<0.01, ***P<0.001. (**N, O**) Left: Barplots showing the proportion of
530 EECs expressing *PYY* in the terminal ileum (**N**) and colon (**O**) in the same cohort of CD patients and
531 controls. Bars represent mean+SD, One-way ANOVA followed by Tukey test, asterisks indicate
532 significant differences *P<0.05, **P<0.01, ***P<0.001. Right: qRT-PCR analysis for *PYY* of ileal
533 tissue from *Tnf*$^{\Delta ARE}$ mice (**N**) and of colonic tissue from IL-10$^{-/-}$ mice (**O**) and respective controls. (**B-**

534 **I, N, O**) Bars represent mean+SD, n≥5 for all groups. Unpaired t tests except (**E**) one-way ANOVA

535 followed by Tukey test. *P* values and r are indicated; a is significantly ($P < 0.05$) different from b.

4.2 Figure2: Inflammation selectively impairs epithelial differentiation but not L cell function

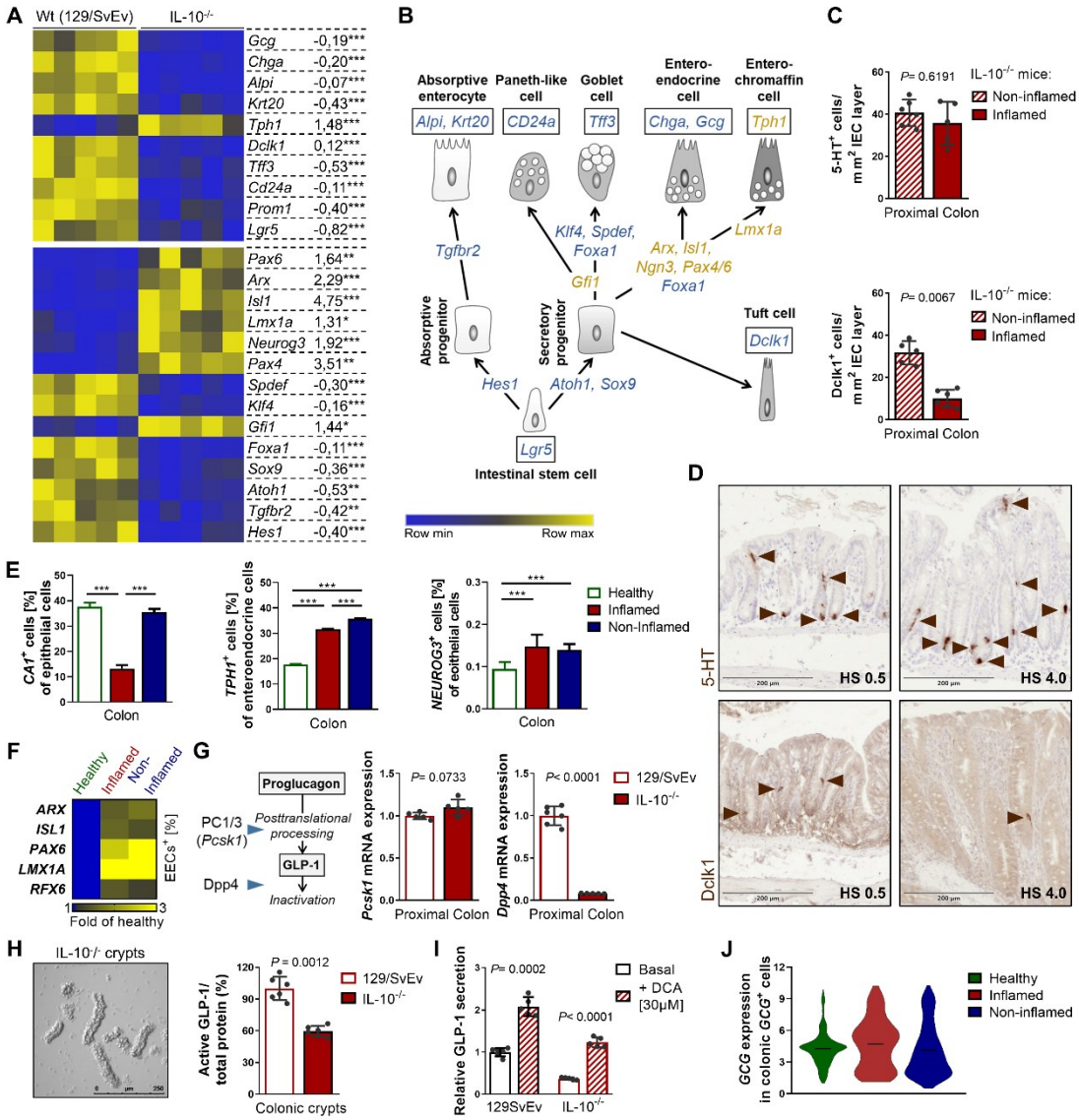

(**A**) Heatmap of a transcriptional profile of isolated intestinal epithelial cells from moderately inflamed (histological score (HS) 2-4) IL-10$^{-/-}$ mice and wild-type (Wt) controls showing marker genes for epithelial subtypes and genes involved in epithelial differentiation. Fold changes in gene expression are given on the right side. Asterisks indicate significant differences **P*<0.05, ***P*<0.01, ****P*<0.001. (**B**) Schematic representation of marker gene expression during differentiation and in epithelial subtypes. Blue = down-regulation, yellow = up-regulation under inflammatory conditions. (**C**) Quantification of 5-HT (serotonin)-positive enterochromaffin cells and Dclk1-positive tuft cells in

545 colonic tissue sections of non-inflamed and inflamed IL-10$^{-/-}$ mice. (**D**) Representative 5-HT and Dclk1
546 IHC stainings for the HS indicated. Arrows indicate cells positive for the respective marker. (**E**)
547 Barplots showing the proportion of epithelial cells expressing *CA1*, a marker gene of mature
548 colonocytes, (left) as well as *TPH1* expression within enteroendocrine cells (middle) in a scRNA-
549 sequencing dataset of colonic intestinal epithelial cells from Crohn´s disease patients (35). Right:
550 proportion of epithelial cells expressing the EEC progenitor marker *NEUROG3*. Bars represent
551 mean+SD. (**F**) Heatmap showing the changes in the proportions of EECs expressing the indicated
552 transcription factors involved in EEC differentiation. $P<0.05$ for all changes shown. One-way ANOVA
553 followed by Tukey test, asterisks indicate significant differences *$P<0.05$, **$P<0.01$, ***$P<0.001$. (**G**)
554 qRT-PCR analysis for *Pcsk1* and *Dpp4*, enzymes regulating GLP-1 abundance (scheme, left), of ileal
555 and colonic tissue from IL-10$^{-/-}$ mice and wild-type (Wt) controls. (**H**) Representative picture of
556 isolated colonic crypts from inflamed IL-10$^{-/-}$ mice (left). Quantification of active GLP-1 (ELISA) in
557 isolated colonic crypts from moderately inflamed IL-10$^{-/-}$ mice and Wt controls (right). (**I**) Basal and
558 deoxycholic acid (DCA)-induced secretion of active GLP-1 from primary colonic organoids derived
559 from IL-10$^{-/-}$ mice and Wt controls. Basal secretion from Wt colonic organoids is set as "1". Bars
560 represent mean+SD, n≥5 for all groups. Unpaired t tests, *P* values and are indicated. (**J**) Violin plot
561 from the same dataset as in (**E**) showing the normalized expression height and distribution of *GCG*
562 within *GCG*-expressing colonic epithelial cells. No significant differences are observed (one-way
563 ANOVA).

564 **4.3 Figure 3: Inflammatory stimuli and microbial structures differentially affect *Gcg* gene**

565 **expression and GLP-1 secretion**

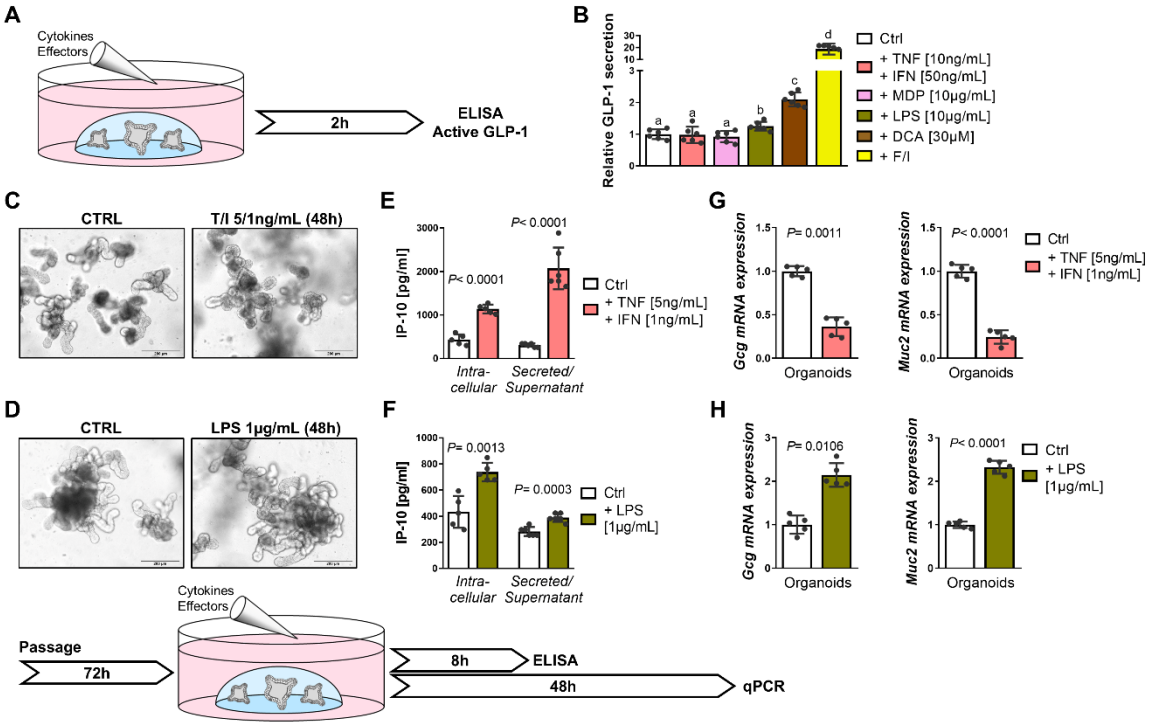

566

567 (**A**) Schematic representation of the experimental setup for (**B**), secretion of active GLP-1 (ELISA)

568 from wild-type (Wt) intestinal organoids stimulated with bacterial-derived Lipopolysaccharide (LPS)

569 or Muramyl dipeptide (MDP), or pro-inflammatory cytokines tumor necrosis factor (TNF) and

570 Interferon gamma (IFN), respectively. Deoxycholic acid (DCA) serves as physiological positive

571 control, forskolin/3-isobutyl-1-methylxanthine (F/I) induces maximal secretion. (**C,D**) Representative

572 pictures of Wt intestinal organoids stimulated with TNF/IFN (**C**) or LPS (**D**) showing no growth

573 impairment and schematic representation of the experimental setup. (**E,F**) Intracellular protein levels

574 and secretion of the pro- inflammatory cytokine IP-10 in Wt intestinal organoids stimulated with (**E**)

575 TNF/IFN or (**F**) LPS, respectively. (**G,H**) qRT-PCR analysis for *Gcg* and *Muc2* of intestinal organoids

576 stimulated with (**G**) TNF/IFN or (**H**) LPS, respectively. (**B, E-H**) Bars represent mean+SD, n≥5 for all

577 groups. Unpaired t tests except (**B**) one-way ANOVA followed by Tukey test. *P* values are indicated;

578 a, b, c, d are significantly ($P < 0.05$) different from each other.

579 **4.4 Figure 4: The inflammation-related metabolic profile is associated with GLP-1^{+} cell loss**

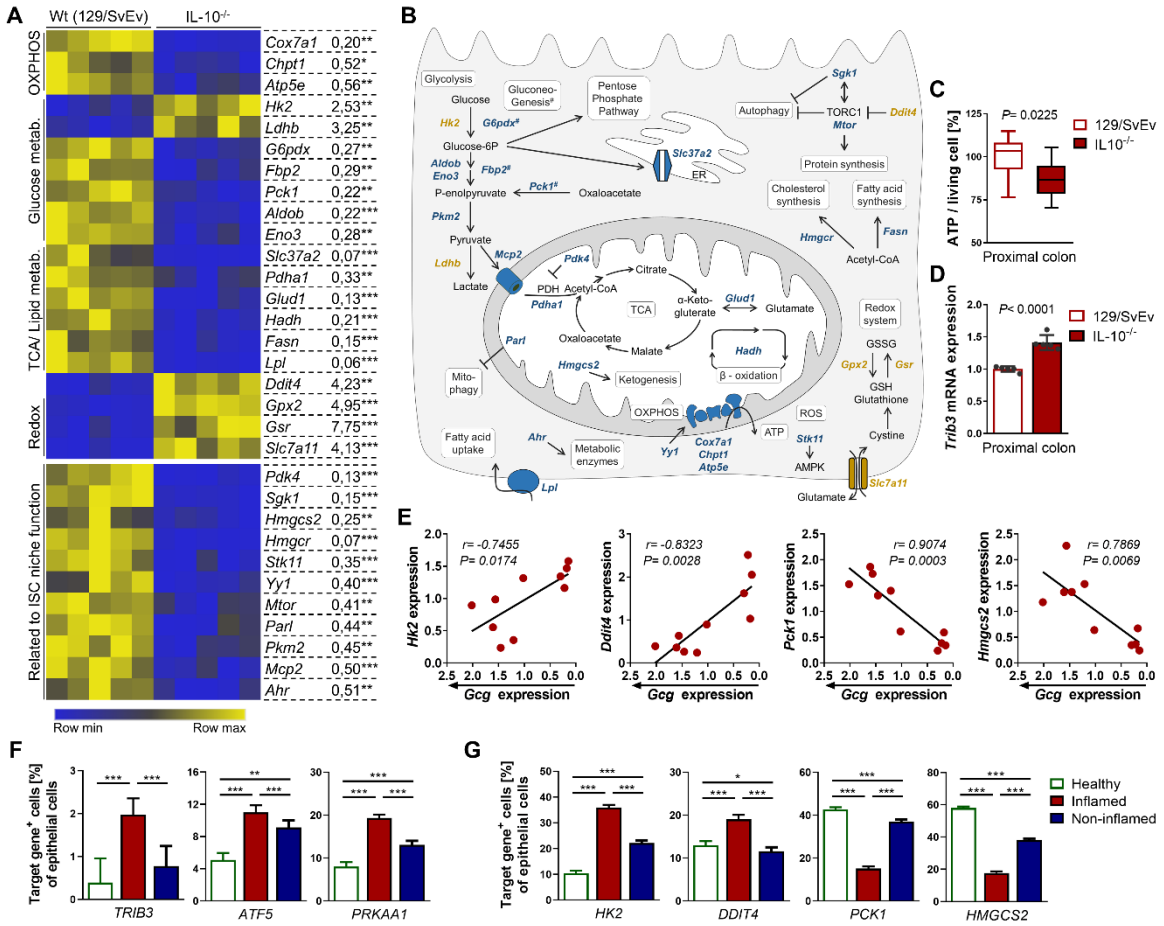

580

581 (**A**) Heatmap of a transcriptional profile of isolated intestinal epithelial cells from moderately inflamed
582 (HS 2-4) IL-10$^{-/-}$ mice and wild-type (Wt) controls showing metabolism-associated genes involved in
583 different metabolic processes and stem cell niche function. Fold changes in gene expression are given
584 on the right side. Asterisks indicate significant differences **P*<0.05, ***P*<0.01, ****P*<0.001. (**B**)
585 Schematic representation of metabolic gene functions. Blue = down-regulation, yellow = up-regulation
586 under inflammatory conditions. (**C**) ATP content of primary isolated colonic crypts from IL-10$^{-/-}$ mice
587 and Wt controls. (**D**) qRT-PCR analysis of isolated colonic epithelial cells for *Trib3*, a marker gene for
588 mitochondrial stress signaling. (**E**) Correlation (Pearson) of metabolic gene expression with *Gcg*
589 mRNA level in colonic epithelial cells isolated from IL-10$^{-/-}$ mice. (**F, G**) Barplots showing the
590 proportion of colonic epithelial cells expressing marker genes for mitochondrial stress signaling

591 (*TRIB3*, *ATF5*) and AMP kinase activation (*PRKAA1*) or (**G**) target metabolic genes in a scRNA-
592 sequencing dataset of colonic intestinal epithelial cells from Crohn´s disease patients (35) and SD of
593 expression. One-way ANOVA followed by Tukey test, asterisks indicate significant differences
594 *P<0.05, **P<0.01, ***P<0.001. Bars represent mean+SD.

595

596 **4.5 Figure 5: Mitochondrial dysfunction impairs epithelial differentiation into L cells**

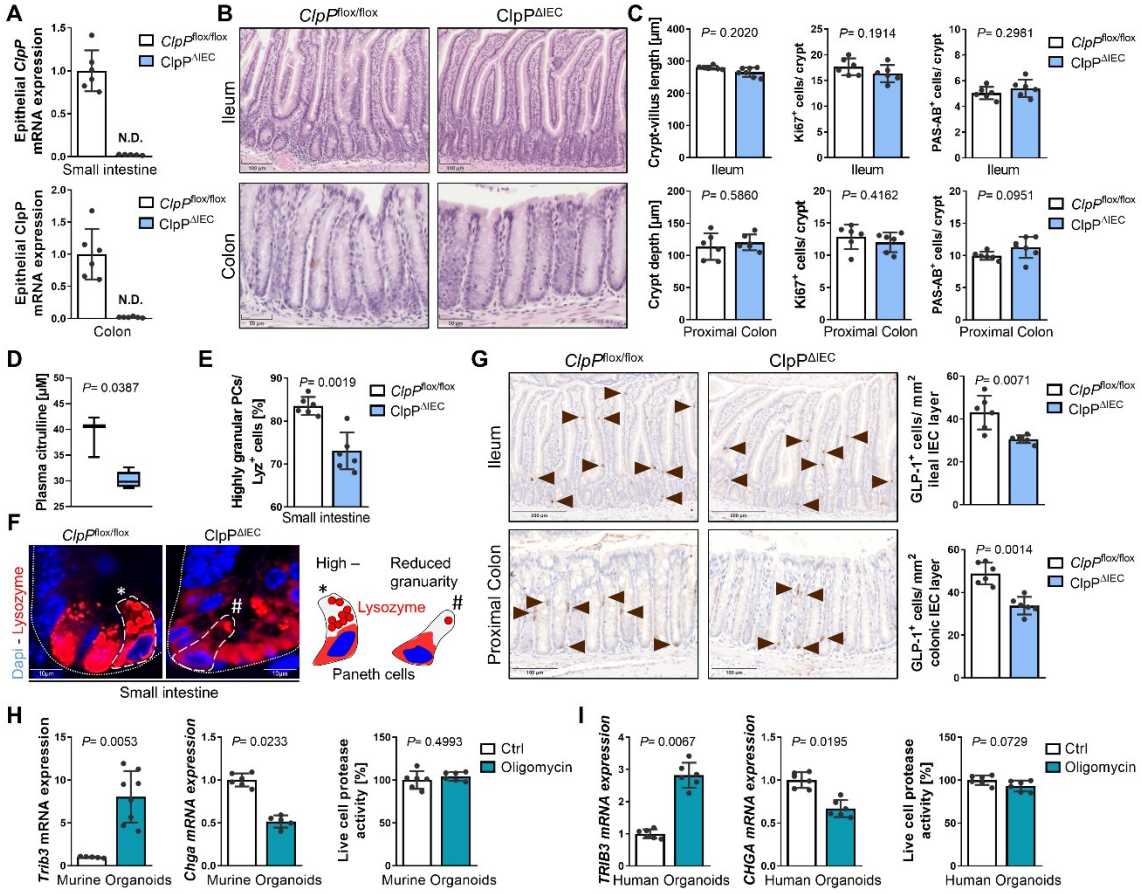

597

598 (**A**) qRT-PCR analysis for *ClpP* in small intestinal and colonic IECs from ClpP$^{\Delta IEC}$ mice and control
599 *ClpP*$^{flox/flox}$ littermates. (**B**) Representative pictures of ileal and colonic tissue sections, and (**C**)
600 quantification of crypt/ villus length (left) actively proliferating cells marked by Ki67 (middle) and
601 mucin-expressing goblet cells (right) in ileal and colonic tissue sections of ClpP$^{\Delta IEC}$ mice and controls.
602 (**D**) Plasma citrulline level of ClpP$^{\Delta IEC}$ mice and controls. (**E**) Quantification of highly granular Lyz^{+}
603 Paneth cells (PC) (≥2 granules) and (**F**) representative immunofluorescence staining of Lysozyme (red)
604 counterstained with Dapi (nuclei, blue) in ClpP$^{\Delta IEC}$ mice and controls including scheme to visualize
605 Paneth cell properties (right). (**G**) Quantification of GLP-1-positive cells and representative pictures
606 of ileal and colonic tissue sections from ClpP$^{\Delta IEC}$ mice and controls immunohistochemically stained
607 for GLP-1. Arrows indicate cells positive for GLP1. (**H**) qRT-PCR analysis of murine intestinal

608 organoids treated with oligomycin (for 6h followed by 18h recovery) for *Trib3* and the enteroendocrine

609 cell marker Chga. *Right*: measurement of living cells in organoid cultures after oligomycin treatment.

610 (**I**) Same analysis as in (**H**) for human organoids. Bars represent mean+SD, n≥5 for all groups.

611 Unpaired t tests, *P* values and are indicated.

612 **4.6 Figure 6: Schematic representation of GLP-1 functions, inflammation-associated epithelial**

613 **alterations and IBD symptoms.**

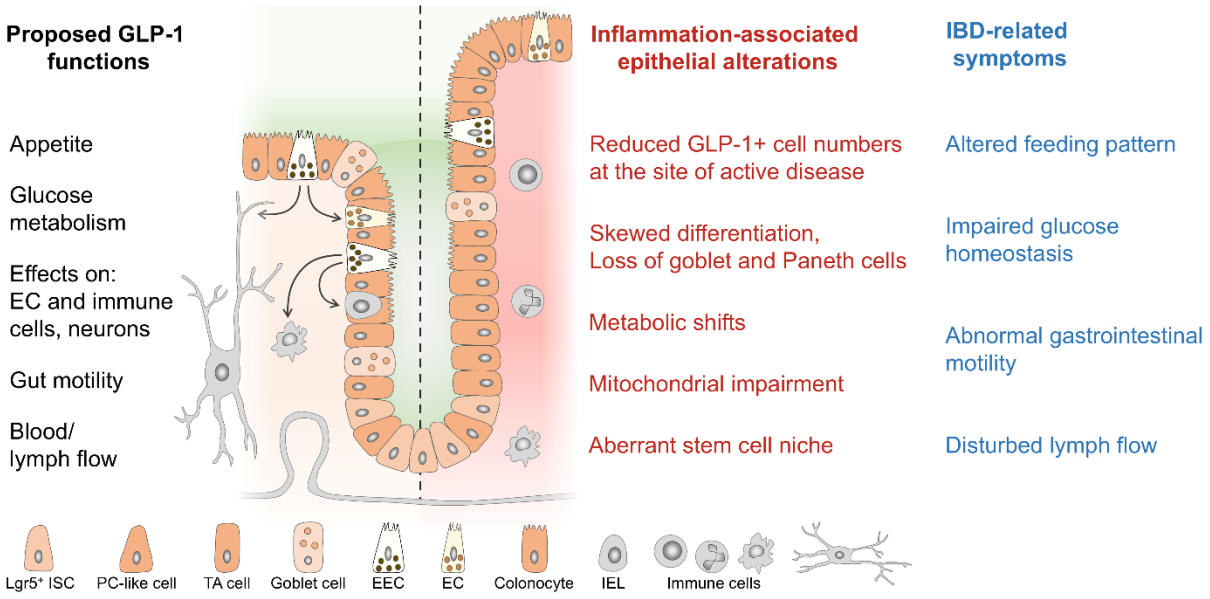

614

615 Schematic representation of GLP-1 functions, inflammation-associated epithelial alterations and IBD

616 symptoms.

617

618 # 5 Methods

619 All authors had access to the study data and had reviewed and approved the final manuscript.

620 ## 5.1 Ethics statement

621 The maintenance and breeding of mouse lines and all experiments were approved by the Institutional
622 Animal Care and Use Committee (IACUC), University of North Carolina at Chapel Hill, NC or
623 approved by the Committee on Animal Health and Care of the local government body of the state of
624 Upper Bavaria (Regierung von Oberbayern; approval numbers 55.2-1-54-2531-164-09, 55.2-1-54-
625 2531-99-13, 55.2-1-54-2532-217-2014) and performed in strict compliance with the EEC
626 recommendations for the care and use of Lab. Anim. (European Communities Council Directive of 24
627 November 1986 (86/609/EEC)). For generation of human organoids, the use of surgically resected
628 human tissue samples was approved by the Ethics Committee of the Medical Faculty of TUM and all
629 participants in this study gave their written informed consent.

630 ## 5.2 Animals

631 In accordance with 3R principles, most samples analyzed in this study for IHC-based quantification of
632 intestinal cells were obtained from our tissue biobank and generated in the context of previously
633 published studies (9, 36-38, 102).

634 **IL-10-deficient (IL-10$^{-/-}$) mice** on 129Sv/Ev background or C57BL/6 background, ***Tnf$^{\Delta ARE}$*** **mice** and
635 **ClpP$^{\Delta IEC}$ mice** were housed (12h light/ dark cycles, 24-26˚C) under specific pathogen-free (SPF)
636 conditions according to the criteria of the Federation for Laboratory Animal Science Associations
637 (FELASA) and bred for several generations in the animal facility. *Tnf$^{\Delta ARE}$* mice were initially provided
638 from Case Western University, Cleveland. *ClpP*$^{flox/flox}$ mice were generated by Taconic-Artemis
639 (Cologne, Germany) in close consultation with our lab, similar to described previously by others(103).
640 To generate epithelial cell-specific ClpP knockout (ClpP$^{\Delta IEC}$) mice, *ClpP*$^{flox/flox}$ mice were crossed to

641 Cre transgenic *Villin1*Cre mice (C57Bl/6N), originally provided by Klaus-Peter Janssen (Klinikum
642 Rechts der Isar, TU München). Mice received a standard chow diet (autoclaved V1124-300; Ssniff,
643 Soest, Germany) and autoclaved water ad libitum. IL-10$^{-/-}$ mice, *Tnf*$^{\Delta ARE}$ mice and Wt littermates were
644 sacrificed at 16-18 weeks of age (9, 36, 37). Male ClpP$^{\Delta IEC}$ mice were analyzed at one year of age.
645 Animals were killed by CO_2 inhalation.

646 **Adoptive T -cell transfer** experiments were performed as previously described (38, 102). Briefly,
647 lymphocyte-deficient SPF 129 SvEv recombination-activating gene (Rag) 2$^{-/-}$ mice were reconstituted
648 at 8 weeks of age by intraperitoneal injection of 5 x 10^5 CD4$^+$ T cells. CD4$^+$ CD25$^-$ and CD4$^+$ CD25$^+$
649 T cells for transfer were obtained from splenocyte suspensions of SPF Wild type mice using a magnetic
650 bead-based CD4$^+$ T cell-isolation kit or the CD4$^+$ CD25$^+$-Regulatory T cell-isolation Kit (Miltenyi
651 Biotec) according to the manufacturer's instructions. 4 weeks later, mice were killed by CO_2 anesthesia
652 followed by cervical dislocation. Reconstitution of mice was confirmed by flow cytometric analysis.
653 Non-reconstituted Rag2$^{-/-}$ mice served as controls.

654 ***Citrobacter rodentium* infection**. The *C. rodentium* strain DBS100 (ATCC 51459; American Type
655 Culture Collection) was used for infection as previously described (104). *C. rodentium* was grown
656 overnight at 37°C in Luria broth. C57BL/6J mice were infected by oral gavage with 0.5 mL of
657 phosphate-buffered saline (PBS) containing approximately 1×10^9 CFU of C. rodentium. To assess the
658 clearance of C. rodentium, fecal pellets were collected from individual mice, homogenized in PBS,
659 serially diluted and plated onto selective MacConkey agar. After an overnight incubation at 37°C,
660 colonies were counted based on the size and distinctive appearance of *C. rodentium* colonies.

661 5.3 **Mouse tissue processing and histopathological analysis**

662 The intestine was removed immediately after euthanization, trimmed free of adjacent tissue and
663 cleaned of stool. Ileal or proximal colonic intestinal tissue was either immediately fixed for preparation

664 of cross sections or cut open and processed as ‘swiss role'. Tissues were fixed in 4% phosphate-buffered
665 formalin for 48h, dehydrated and embedded in paraffin (FFPE). For histopathological assessment, 5 µm
666 sections were stained with hematoxylin (of Mayer) and 0.2% eosin (ethanolic solution; both Medite)
667 in an automated staining machine (Leica). Images were acquired by a PreciPoint M8 microscope
668 (Precipoint). Ileal and colonic sections were blindly assessed for mononuclear cell infiltration into
669 lamina propria, crypt hyperplasia, goblet cell depletion and ulcer formation resulting in a score from 0
670 (not inflamed) to 12 (highly inflamed) as described previously (48).

671 5.4 **Morphometric measurements of intestinal tissues**

672 The crypt depth and number of crypts per area were analyzed in H&E stainings of intestinal tissue
673 sections. In fifty well-oriented crypts, the length from the crypt base to the crypt top or villus tip,
674 respectively, was measured using the ViewPoint Light software, and the average length was calculated
675 for each section. To determine the number of crypts per 100µm, the number of crypts within 100µm
676 intestinal tissue length was counted in well oriented tissue areas using the ViewPoint Light software.

677 5.5 **Alcian blue / Periodicacid-Schiff (PAS-AB) staining and quantification of goblet cells**

678 FFPE tissue sections were deparaffinized, rehydrated, and stained with alcian blue (Fisher, Dreieich,
679 Germany) for detection of acidic mucins (0.5% v/v in 3% acetic acid, pH=2.5, 5 min) in goblet cells.
680 Sections were then treated with periodic acid (0.5% v/v, 10 min) and co-stained with Schiff’s reagent
681 (Sigma- Aldrich, Taufkirchen, Germany) for neutral mucins (15 min). Nuclei were counterstained with
682 hematoxylin, and tissue sections were dehydrated and mounted with DPX new (Merck KGaA,
683 Darmstadt, Germany). Slides were scanned and further analyzed using a PreciPoint M8 microscope
684 (Precipoint, Freising, Germany). The number of goblet cells was counted based on Alcian
685 blue/Periodicacid-Schiff (PAS-AB) staining. Fifty well-oriented crypts were selected per mouse, and
686 PAS^+ cells were counted. The number of PAS^+ cells was calculated per crypt/ per mouse.

687 5.6 **Immunohistochemistry**

688 Immunohistochemical (IHC) stainings were performed on 5 µm FFPE tissue sections as described
689 previously (64). Briefly, FFPE tissue sections were deparaffinized and rehydrated in an automated
690 staining machine (Leica). After heat-mediated antigen retrieval (boiling in 10mM citrate buffer (pH=6)
691 in a microwave (23min; 900 watt)), sections were incubated for 10min with 3% H_20_2 (Sigma-Aldrich).
692 Subsequently, sections were blocked, and a primary antibody was applied overnight at 4°C. After
693 several washing steps, sections were incubated with the secondary antibody (horseradish peroxidase
694 coupled; 1h, room temperature). Antigen detection was performed using 3,3′-diaminobenzidine (DAB)
695 or enhanced DAB (Sigma Aldrich), and nuclei were counterstained with hematoxylin. Slides were
696 mounted with xylol-based mounting medium (Roti®-Histokitt). Stainings were scanned and using a
697 PreciPoint M8 microscope (Precipoint). Antibodies and dilutions are given in **Table 1 and 2**.

698 5.7 **Immunofluorescence stainings and Paneth cell phenotype quantification**

699 Immunofluorescence stainings for lysozyme were performed on 4 µm FFPE tissue sections as
700 described previously(9). Antibodies used were: Anti-Lysozyme Rabbit Dako, Agilent, Santa Clara
701 (1:1000), Alexa Fluor donkey anti rabbit 546 Life Technologies, Carlsbad, CA (1:200) and Dapi to
702 counterstain nuclei, Sigma- Aldrich, Taufkirchen, Germany (1:1000). Stainings were visualized using
703 the Flouview FV10i microscope (Olympus, Shinjuku, Japan). Lysozyme positive cells numbers were
704 determined in ileal tissue sections. To assess the granularity of Lyz positive cells, all PCs contained in
705 50 well oriented crypts were analyzed. Lyz positive cells were considered as highly granular if ≥2 Lyz
706 positive granules were visible within the cell. The quantification was performed in a blinded manner.

707 5.8 **Quantification of cell numbers**

708 At least three non-consecutive sections from each mouse were used for quantification of GLP-1, Dclk1,
709 Ki67 or 5-HT positive cells. Well-oriented (visible open crypts/ crypt-villus axis) tissue areas were

710 selected and epithelial cells positive for the respective marker were counted. The number of positive
711 cells was calculated over the total epithelial area quantified using the ViewPoint Light software
712 (Precipoint). For individual mice, the number of positive cells was calculated as mean of quantified
713 sections and areas. For quantification of Ki67 expressing cells, cells positive for Ki67 were counted in
714 50 well-oriented crypts per mouse and the average number of Ki67 positive cells was calculated per
715 crypt/ per mouse. The quantification was performed in a blinded manner.

716 5.9 **Isolation of primary IECs**

717 Primary IECs were purified as previously described (64). Approximately 6 cm of intestine were
718 inverted on a needle, vortexed vigorously and incubated (37 °C, 15 min) in DMEM containing 10%
719 fetal calf serum (Biochrom), 1.0% Glutamine, 0.8% antibiotics/antimycotics (all Sigma-Aldrich)
720 supplemented with 1 mM dithiothreitol (Roth). The IEC suspension was centrifuged (7 min, 300*g*, RT)
721 and the cell pellet was re-suspended in DMEM containing fetal calf serum, l-glutamine and antibiotics.
722 The remaining tissue was incubated in 20 ml PBS (10 min, 37 °C) containing 1.5 mM EDTA (Roth).
723 After vortexing, the tissue was discarded and the cell suspension from this step was centrifuged as
724 mentioned above. Cells obtained in both steps were combined and primary IECs were purified by
725 centrifugation through a 20%/40% discontinuous Percoll gradient (GE Healthcare) at 600*g* for 30 min.
726 IECs were immediately snap frozen.

727 5.10 **Primary crypt isolation and intestinal organoid culture**

728 Primary intestinal crypts from mouse (ileum, colon) and human (from macroscopically healthy tissue
729 of surgical specimen of the ileum) were isolated by tissue incubation in 2mM EDTA (Fisher) or Gentle
730 Cell Dissociation Reagent (STEMCELL Technologies), respectively, and cultured as described
731 elsewhere (64, 105, 106). For organoid culture, murine crypts were embedded in 25µl matrigel (BD
732 Biosciences) and cultured in 48 well plates. Murine organoids were grown in crypt culture medium

733 (CCM), advanced DMEM/F12 medium (Gibbco) containing 2 mM GlutaMax (Gibbco), 10 mM
734 HEPES, penicillin, streptomycin and amphotericin (all Sigma- Aldrich) supplemented with N2, B27
735 (both Gibbco), 1 mM N-acetylcystein (Sigma- Aldrich), 50 µg/mL EGF (ImmunoTools), 100 µg/mL
736 noggin and 0.5 µg/mL R-spondin 1 (both PeproTec) or, when derived from colonic crypts, in Murine
737 Intesticult medium (STEMCELL Technologies). For human organoid culture, 500 crypts were
738 embedded in 30µl matrigel (BD Biosciences) per well, resulting in approx. 100 mature organoids, and
739 cultured in 48 well plates. Human organoids were cultivated in Human Intesticult medium
740 (STEMCELL Technologies) containing Wnt factors.

741 5.11 **Intestinal organoid stimulation**

742 For assessing the GLP-1 secretory capacity of IL-10$^{-/-}$ enteroendocrine cells, primary colonic crypts
743 were embedded in matrigel and cultured for 48h prior to stimulation to retain the inflammatory
744 phenotype. For other experiments, murine and human organoids were used 4 to 6 days after passaging.
745 Two days prior to the start of experiments, medium of human organoids was changed to CCM to reduce
746 stem niche factors (106). When indicated, organoids were stimulated with TNF (5ng/mL) and IFN (1
747 ng/mL) or LPS (1µg/mL) for 48h, or treated with 2.5µM oligomycin (Sigma- Aldrich) for 6h and
748 subsequently cultured in CCM for 18h, for gene expression analysis to assess differentiation. To
749 measure IP-10 production and secretion, organoids were stimulated with TNF/ IFN or LPS in the same
750 concentrations for 24h. To measure GLP-1 secretion, organoids were washed four times with HEPES-
751 saline buffer (pH 7.4) containing BSA and DPP4 inhibitor. Subsequently, organoids were incubated
752 for 2h in HEPES-saline buffer supplemented with either LPS (10µg/mL), MDP (10µg/mL), a
753 combination of TNF (10ng/mL) and IFN (50 ng/mL), DCA (30 µM) (as physiological positive control),
754 or a mixture of 10 µM Forskolin and 10 µM 3-isobutyl-1-methylxanthine (F/I, for maximal hormone
755 output).

756 5.12 **GLP-1 measurements**

757 Organoid culture: after stimulation, the culture plate was placed on ice, supernatants were collected
758 and immediately cold PBS was added to the organoid cultures. Supernatant samples were centrifuged
759 (400 g) for 5 min at 4 °C and the supernatant was snap-frozen in liquid nitrogen. Organoids including
760 Matrigel were resuspended in cold PBS and washed twice by centrifugation (600 g) for 10 min at 4 °C.
761 The organoid pellet was dissolved in lysis buffer containing 150 mM NaCl, 50 mM Tris-HCl, 1%
762 Igepal CA-630, 0.5% DCA and a protease inhibitor mix, for 20 min at 37 °C, and centrifuged (600 g)
763 for 10 min at 4 °C. The supernatant was collected and snap-frozen. Primary crypts were lysed and
764 processed accordingly. All samples were kept at −80 °C until analysis of incretin hormones. GLP-1
765 concentrations in supernatant and lysate were quantified using a Glucagon-Like Peptide 1 (Active)
766 ELISA kit (Millipore). The amount of GLP-1 secreted by the cultures was calculated as a percentage
767 of the GLP-1 content (secreted plus intracellular) and normalized to basal secretion. The content of
768 active GLP-1 in primary crypts was normalized to total protein content (determined by Bradford assay)
769 of samples and calculated as percentage of Wt (129/SvEv) colonic crypts.

770 5.13 **IP-10 measurements**

771 After stimulation, supernatants and organoids were collected according to the procedures described for
772 GLP-1 measurement. The organoids were dissolved using a non-denaturating lysis buffer containing
773 PMSF and a protease inhibitor mix. IP-10 concentrations were determined using an IP-10 ELISA kit
774 (R&D Systems) according to the manufacturer's instructions.

775 5.14 **Measurement of living cells and cellular ATP content**

776 Life- and dead- cell protease activity was measured using the MultiTox-Fluor Cytotoxicity Assay and
777 ATP content was determined using the CellTiter-Glo Luminescent Cell Viability Assay (both from
778 Promega), according to the manufacturer's instructions. Fluorescence and luminescence were

779 measured using the Tecan infinite M200 (Tecan Group Ltd.) and the i-control™ Microplate Reader
780 software (Tecan).

781 5.15 **Measurement of plasma citrulline**

782 EDTA blood was taken during sampling from venacava. Quantitation of amino acids in EDTA plasma
783 was performed using LC–MS/MS with aTRAQ labelling (aTRAQ reagent kit 4442671, AB SCIEX,
784 Framingham, MA, USA). Quantitation was done according to the manufacturer's instructions using
785 40 µl of serum sample. The analysis was performed on a triple quadrupole QTRAP3200 LC–MS/MS
786 system (AB SCIEX) coupled to an Agilent 1260 Infinity Quaternary LC Pump (Agilent, Santa Clara,
787 CA, USA).

788 5.16 **RNA isolation, reverse transcription and quantitative real-time PCR**

789 For mRNA isolation from primary IEC or organoids, the NucleoSpin RNAII kit (Macherey-Nagel)
790 was used according to the manufacturer's instructions. In the case of organoid culture, matrigel
791 containing organoids was directly dissolved in RA1 buffer. Reverse transcription was performed as
792 previously described (107). Quantitative Real-time PCR (qRT–PCR) was performed using the Light
793 Cycler 480 system (Roche Diagnostics) and applying the Universal Probe Library system according to
794 the manufacturer's instructions. Primer sequences and probes are given in **Table 3**. Relative induction
795 of gene mRNA expression was calculated based on Ct values using the expression of house-keeping
796 genes *HPRT*/*Hprt* for normalization. Data are expressed as fold change over controls.

797 5.17 **Single-cell RNA sequencing and data visualization**

798 The single-cell RNA sequencing dataset comprising intestinal epithelial cells from the terminal ileum
799 and colon of healthy donors as well as inflamed and non-inflamed tissues from Crohn´s disease patients
800 was obtained from the Human Cell Atlas portal

801 (https://explore.data.humancellatlas.org/projects/cae461de-ecbd-482f-a5d4-11d607fc12ba) and
802 initially published by Kong et al. (35). This data set comprises 720,633 cells across 71 donors with
803 various inflammation statuses. We used pre-processed Seurat objects provided by the original authors,
804 which included normalization, dimensionality reduction, and clustering. Analysis was performed in R
805 (v4.3.3) using Seurat (v5.1.0). Cell type annotations and UMAP embeddings were directly extracted
806 from the metadata. Ensembl gene IDs were converted to gene symbols using biomaRt (v2.58.2).
807 Subsets of enteroendocrine cells were generated based on cell type annotations, and UMAP plots were
808 used to visualize marker gene expression (e.g., *GCG*). For each subset, we calculated the proportion of
809 cells expressing target genes (e.g., mitochondrial stress markers, metabolic genes) and computed
810 average expression levels by inflammation status (healthy, inflamed, and non-inflamed), including
811 standard deviation, sample size, and standard error of the mean. The complete analysis code is available
812 at: https://github.com/Kate0107/scRNAseq-analysis-of-GLP-1-secreting-enteroendocrine-cells-in-
813 the-context-of-intestinal-inflammation/blob/main/GLP1.R.

814 5.18 **Statistical analysis and heatmap generation**

815 Heatmaps were generated using Morpheus (https://software.broadinstitute.org/morpheus) or GraphPad
816 Prism (GraphPad). Statistical analysis was performed using GraphPad Prism. Statistical tests used
817 were: unpaired t-test for two group-comparisons or chi-square test or One-Way analysis of variances
818 (ANOVA) followed by an appropriate multiple comparison procedure for comparisons comprising
819 more than two groups. Correlation analysis was performed according to Pearson test. Data are
820 expressed as mean ± SD, $n \geq 5$ for all groups. Differences between groups were considered significant
821 if P-values were < 0.05.

822 **Table 1: Primary antibodies used for IHC**

Antibody	Species	Company	Dilution
Anti-Dclk1	Rabbit	Biomol	1:100
Anti-GLP-1	Rabbit (2760S)	CST	1:200
Anti-Ki67	Rabbit (D3B5)	CST	1:300
Anti-Serotonin (5-HT)	Rat (ab6336)	Abcam	1:150

823

824 **Table 2: Secondary antibodies used for IHC**

Antibody	Company	Dilution
HRP conjugated donkey anti rabbit IgG	Dianova (711-035-152)	1:300
HRP conjugated goat anti rat IgG	Dianova (112-035-003)	1:300

825

826 **Table 3: Primer sequences and probes**

	Mouse		
Target genes	**Forward primer**	**Reverse primer**	**Probe**
Ahr	gcaagaaggagagttcttgttacag	aaagcccaggtaatcttggata	69
Aldob	cgtgctgtgttgaggattgc	atagcgagccagagcattgg	11
Alpi	catctccaacatggacattga	ggttccagactggttactgtca	109
Atoh1	gggttgtagtggacgagctt	gcttctgtaccccattcacc	11
Atp5e	cggttttcccagatctgtgc	cccgaagtcttctcagcgtt	112
Arx	caggagagaggagcagaggt	actgattgctcatggctggt	117
Cck	tgatttccccatccaaagc	gcttctgcagggactaccg	9
Cd24a	ctggggttgctgcttctg	caacagatgtttggttgcagtaa	68
ChgA	ggaggctgtggctacacaca	ccatccactgcctgagagtc	89
Chpt1	aggaggcaccatactggaca	tcccatcaatggcatccagt	95
Cox7a1	gctcatctaccagaagccact	gtcattgtcggcctggaaga	53
Ddit4	ccagagaagagggccttga	ccatccaggtatgaggagtctt	80
Dclk1	ttcaacacaggccccaag	ccttatcaagagcggtggtt	18
Dpp4	tgggaacactggaagttgaa	cgcttgctatccacaaatcc	71
Eno3	acaaagcacgatacctgggg	ttccagcagagcaggaccta	161
Fasn	cccaccctgatttctgccat	cacctaggccaccagtgatg	23
Fbp2	tgcaggtgtgtcttcaacga	gcctccctttgctccttgta	74
Foxa1	acagggttggatggttgtgt	tgctctcatgcccttccatc	36
Gcg	ccagtgatgtgagttcttacttgg	caatggcgacttcttctgg	27
Gfi1	atcaagcctgccacgagaag	ctcctctgatggcaccacag	9
Gip	tctcagggaaaggaggacaa	tcagcacatcatcatcactgag	98
Glud1	atcaagccctgcaaccatgt	tagccttcgatgacctccca	60
Gpx2	gttctcggcttcccttgc	ttcaggatctcctcgttctga	2
Gsr	ccaaggtggcctcaaacaac	gcaggcctagaattccagca	78
G6pdx	gagccacccatctttccaca	aggggcagactgataggcat	11

827 Table 3 continued

Mouse			
Target genes	**Forward primer**	**Reverse primer**	**Probe**
Hadh	tggatactacaaagttcatcttgga	aaggactgggctgaaataagg	106
Hes1	acaccggacaaaccaaagac	cgcctcttctccatgatagg	99
Hk2	ttcaccttctccttcccttg	ccctttgtccacttgaggag	64
Hmgcr	tgattggagttggcaccat	tggccaacactgacatgc	78
Hmgcs2	gtaacggggagcactgagag	ccaaccgtttccatacccca	110
Hprt	tcctcctcagaccgctttt	cctggttcatcatcgctaatc	95
Isl1	tgccctgtagctggtttctc	gaaataaagaaaaggaaagaaaaaggat	91
Klf4	ctgaaggcgtctctgaccac	cgtctgggcttcctttgcta	66
Krt20	ggttcaagtcacggagctga	ttcatgctgaggtgggactg	80
Ldhb	ggcagagaagcttggcatt	agactcctgccacattcacc	3
Lgr5	cttcactcggtgcagtgct	cagccagctaccaaataggtg	60
Lmx1a	ctcaccccgaacatgttgga	ccgaggtctcaatcgcactt	25
Lpl	ctcgctctcagatgccctac	ggttgtgttgcttgccatt	95
Lyz1	ggcaaaaccccaagatctaa	tctctcaccaccctctttgc	46
Mcp2	cactgtgttgatggctacagg	caaatccgaaacagctgagag	18
Mtor	tctggtaactgaggcctgga	gtccactggaagcacagaca	52
Muc2	ggcagtacaagaaccggagt	ggtctggcagtcctcgaa	66
Neurog3	aaactccaaagggtggatga	tgtgccagcctctgacttag	93
Parl	tgcatcgggagcaatcatga	atgatagcgagcctcccctc	112
Pax4	ctctgtgaagctctggaccc	gtttgctggtggtctggtct	78
Pax6	ttgcataagaggcatcggct	cagcaccgaaagcaagacac	78
Pck1	aaatgctttgcgttgcggat	tgcccaggatcagcatatgc	69
Pcsk1	tggagttgcatataattccaaagtt	agcctcaatggcatcagttac	42
Pdha1	catcgttggagctcaggtg	cgccgtataatgtcaaacagac	15
Pdk4	cgcttagtgaacactccttcg	cttctgggctcttctcatgg	22
Pkm2	gcaggaaccgaagtacgc	tgtgttccaggaaggtgtca	3
Prom1	cagcggcagaagcagaat	tggttagccacaaagccata	69
Pyy	cctaccctgccaaaccag	ggacatctctttttccataccg	17
Sgk1	acacgctgaagttcagtcca	aggagaggggttagcgttca	92
Slc37a2	tgctgcatcatgctgatctt	cccattctggccaatgtagt	32
Slc7a11	tgggtggaactgctcgtaat	aggatgtagcgtccaaatgc	1
Sox9	gtacccgcatctgcacaac	ctcctccacgaagggtctct	66
Spdef	cctcctggtccctgaggt	cagtgaatgtggccctgac	40
Stk11	cttcatccaccgcatcgact	tcaggtacttgccgatgagc	28
Tff3	gtaacaaccgtggctgctg	gagcctggacagcttcaaaa	109
Tgfbr2	tggctctggtactctgggaa	gaaccaaatgggggctcgta	7
Tph1	ggctatcgggaagacaacat	cggatggaaaacccagtg	88
Trib3	gtcgctttgtcttcagcaact	tcatctgatccagtcatcacg	67
Yy1	ctggagaaaagccctttcag	gtcgaaggggcacacatag	94

Human			
Target genes	**Forward primer**	**Reverse primer**	**Probe**
HPRT1	tgatagatccattcctatgactgtaga	caagacattcttccagttaaagt	22
LGR5	accagactatgcctttggaaac	tcccagggagtggattctatt	78
TRIB3	gtcttcgctgaccgtgaga	cagtcagcacgcaggagtc	67

828

829

830 **6 References**

831 1. Zietek T, Daniel H. Intestinal Nutrient Sensing and Blood Glucose Control. *Current opinion*
832 *in clinical nutrition and metabolic care* (2015) 18(4):381-8. Epub 2015/05/24. doi:
833 10.1097/MCO.0000000000000187.

834 2. Worthington JJ. The Intestinal Immunoendocrine Axis: Novel Cross-Talk between
835 Enteroendocrine Cells and the Immune System During Infection and Inflammatory Disease.
836 *Biochemical Society transactions* (2015) 43(4):727-33. Epub 2015/11/10. doi:
837 10.1042/BST20150090.

838 3. Clavel T, Haller D. Bacteria- and Host-Derived Mechanisms to Control Intestinal Epithelial
839 Cell Homeostasis: Implications for Chronic Inflammation. *Inflamm Bowel Dis* (2007) 13(9):1153-64.
840 Epub 2007/05/04. doi: 10.1002/ibd.20174.

841 4. Helander HF, Fandriks L. Surface Area of the Digestive Tract - Revisited. *Scandinavian*
842 *journal of gastroenterology* (2014) 49(6):681-9. Epub 2014/04/04. doi:
843 10.3109/00365521.2014.898326.

844 5. Barker N. Adult Intestinal Stem Cells: Critical Drivers of Epithelial Homeostasis and
845 Regeneration. *Nat Rev Mol Cell Biol* (2014) 15(1):19-33. doi: 10.1038/nrm3721.

846 6. Barker N, Clevers H. Leucine-Rich Repeat-Containing G-Protein-Coupled Receptors as
847 Markers of Adult Stem Cells. *Gastroenterology* (2010) 138(5):1681-96. doi:
848 10.1053/j.gastro.2010.03.002.

849 7. Sartor RB. Mechanisms of Disease: Pathogenesis of Crohn's Disease and Ulcerative Colitis.
850 *Nat Clin Pract Gastroenterol Hepatol* (2006) 3(7):390-407.

851 8. Cadwell K, Liu JY, Brown SL, Miyoshi H, Loh J, Lennerz JK, et al. A Key Role for
852 Autophagy and the Autophagy Gene Atg16l1 in Mouse and Human Intestinal Paneth Cells. *Nature*
853 (2008) 456(7219):259-63. doi: 10.1038/nature07416.

854 9. Khaloian S, Rath E, Hammoudi N, Gleisinger E, Blutke A, Giesbertz P, et al. Mitochondrial
855 Impairment Drives Intestinal Stem Cell Transition into Dysfunctional Paneth Cells Predicting
856 Crohn's Disease Recurrence. *Gut* (2020) 69(11):1939-51. Epub 20200228. doi: 10.1136/gutjnl-2019-
857 319514.

858 10. Wang H, Steeds J, Motomura Y, Deng Y, Verma-Gandhu M, El-Sharkawy RT, et al. Cd4+ T
859 Cell-Mediated Immunological Control of Enterochromaffin Cell Hyperplasia and 5-
860 Hydroxytryptamine Production in Enteric Infection. *Gut* (2007) 56(7):949-57. doi:
861 10.1136/gut.2006.103226.

862 11. Worthington JJ, Samuelson LC, Grencis RK, McLaughlin JT. Adaptive Immunity Alters
863 Distinct Host Feeding Pathways During Nematode Induced Inflammation, a Novel Mechanism in
864 Parasite Expulsion. *PLoS Pathog* (2013) 9(1):e1003122. doi: 10.1371/journal.ppat.1003122.

865 12. Gerbe F, Sidot E, Smyth DJ, Ohmoto M, Matsumoto I, Dardalhon V, et al. Intestinal
866 Epithelial Tuft Cells Initiate Type 2 Mucosal Immunity to Helminth Parasites. *Nature* (2016)
867 529(7585):226-30. doi: 10.1038/nature16527.

868 13. van der Post S, Jabbar KS, Birchenough G, Arike L, Akhtar N, Sjovall H, et al. Structural
869 Weakening of the Colonic Mucus Barrier Is an Early Event in Ulcerative Colitis Pathogenesis. *Gut*
870 (2019) 68(12):2142-51. Epub 20190326. doi: 10.1136/gutjnl-2018-317571.

871 14. Rath E, Haller D. Intestinal Epithelial Cell Metabolism at the Interface of Microbial
872 Dysbiosis and Tissue Injury. *Mucosal Immunol* (2022) 15(4):595-604. Epub 20220509. doi:
873 10.1038/s41385-022-00514-x.

874 15. Rath E, Moschetta A, Haller D. Mitochondrial Function - Gatekeeper of Intestinal Epithelial
875 Cell Homeostasis. *Nat Rev Gastroenterol Hepatol* (2018) 15(8):497-516. doi: 10.1038/s41575-018-
876 0021-x.

877 16. Urbauer E, Rath E, Haller D. Mitochondrial Metabolism in the Intestinal Stem Cell Niche-
878 Sensing and Signaling in Health and Disease. *Front Cell Dev Biol* (2020) 8:602814. Epub 20210105.
879 doi: 10.3389/fcell.2020.602814.

880 17. Ludikhuize MC, Meerlo M, Gallego MP, Julià MB, Nguyen NTB, Brombacher EC, et al.
881 Mitochondria Define Intestinal Stem Cell Differentiation Downstream of a Foxo/Notch Axis. *bioRxiv*
882 (2019):777391. doi: 10.1101/777391.

883 18. Haberman Y, Karns R, Dexheimer PJ, Schirmer M, Somekh J, Jurickova I, et al. Ulcerative
884 Colitis Mucosal Transcriptomes Reveal Mitochondriopathy and Personalized Mechanisms
885 Underlying Disease Severity and Treatment Response. *Nat Commun* (2019) 10(1):38. doi:
886 10.1038/s41467-018-07841-3.

887 19. Mottawea W, Chiang CK, Muhlbauer M, Starr AE, Butcher J, Abujamel T, et al. Altered
888 Intestinal Microbiota-Host Mitochondria Crosstalk in New Onset Crohn's Disease. *Nat Commun*
889 (2016) 7:13419. doi: 10.1038/ncomms13419.

890 20. Denson LA. Mitochondrial Networks: A New Therapeutic Target in Colitis. *Cell Mol*
891 *Gastroenterol Hepatol* (2020) 10(2):426-7. doi: 10.1016/j.jcmgh.2020.05.008.

892 21. Mancini NL, Goudie L, Xu W, Sabouny R, Rajeev S, Wang A, et al. Perturbed Mitochondrial
893 Dynamics Is a Novel Feature of Colitis That Can Be Targeted to Lessen Disease. *Cell Mol*
894 *Gastroenterol Hepatol* (2020) 10(2):287-307. doi: 10.1016/j.jcmgh.2020.04.004.

895 22. Rath E, Haller D. Mitochondria at the Interface between Danger Signaling and Metabolism:
896 Role of Unfolded Protein Responses in Chronic Inflammation. *Inflamm Bowel Dis* (2012)
897 18(7):1364-77. doi: 10.1002/ibd.21944.

898 23. Jackson DN, Theiss AL. Gut Bacteria Signaling to Mitochondria in Intestinal Inflammation
899 and Cancer. *Gut Microbes* (2020) 11(3):285-304. doi: 10.1080/19490976.2019.1592421.

900 24. Friedrich M, Diegelmann J, Schauber J, Auernhammer CJ, Brand S. Intestinal
901 Neuroendocrine Cells and Goblet Cells Are Mediators of Il-17a-Amplified Epithelial Il-17c
902 Production in Human Inflammatory Bowel Disease. *Mucosal Immunol* (2015) 8(4):943-58. doi:
903 10.1038/mi.2014.124.

904 25. Sakiyama T, Fujita H, Tsubouchi H. Autoantibodies against Ubiquitination Factor E4a
905 (Ube4a) Are Associated with Severity of Crohn's Disease. *Inflammatory bowel diseases* (2008)
906 14(3):310-7. doi: 10.1002/ibd.20328.

907 26. Zietek T, Rath E. Inflammation Meets Metabolic Disease: Gut Feeling Mediated by Glp-1.
908 *Front Immunol* (2016) 7:154. Epub 20160422. doi: 10.3389/fimmu.2016.00154.

909 27. Massironi S, Zilli A, Cavalcoli F, Conte D, Peracchi M. Chromogranin a and Other
910 Enteroendocrine Markers in Inflammatory Bowel Disease. *Neuropeptides* (2016) 58:127-34. Epub
911 20160112. doi: 10.1016/j.npep.2016.01.002.

912 28. Hadjiyanni I, Siminovitch KA, Danska JS, Drucker DJ. Glucagon-Like Peptide-1 Receptor
913 Signalling Selectively Regulates Murine Lymphocyte Proliferation and Maintenance of Peripheral
914 Regulatory T Cells. *Diabetologia* (2010) 53(4):730-40.

915 29. Yusta B, Baggio LL, Koehler J, Holland D, Cao X, Pinnell LJ, et al. Glp-1r Agonists
916 Modulate Enteric Immune Responses through the Intestinal Intraepithelial Lymphocyte Glp-1r.
917 *Diabetes* (2015) 64(7):2537-49. Epub 2015/03/05. doi: 10.2337/db14-1577.

918 30. Moran GW, Leslie FC, McLaughlin JT. Crohn's Disease Affecting the Small Bowel Is
919 Associated with Reduced Appetite and Elevated Levels of Circulating Gut Peptides. *Clin Nutr* (2013)
920 32(3):404-11. Epub 2012/09/25. doi: 10.1016/j.clnu.2012.08.024.

921 31. Keller J, Binnewies U, Rosch M, Juul Holst J, Beglinger C, Andresen V, et al. Gastric
922 Emptying and Disease Activity in Inflammatory Bowel Disease. *European journal of clinical*
923 *investigation* (2015). Epub 2015/10/02. doi: 10.1111/eci.12542.

924 32. El-Salhy M, Hatlebakk JG. Changes in Enteroendocrine and Immune Cells Following Colitis
925 Induction by Tnbs in Rats. *Mol Med Rep* (2016) 14(6):4967-74. Epub 20161031. doi:
926 10.3892/mmr.2016.5902.

927 33. El-Salhy M, Umezawa K, Hatlebakk JG, Gilja OH. Abnormal Differentiation of Stem Cells
928 into Enteroendocrine Cells in Rats with Dss-Induced Colitis. *Mol Med Rep* (2017) 15(4):2106-12.
929 Epub 20170301. doi: 10.3892/mmr.2017.6266.

930 34. Zatorski H, Salaga M, Zielinska M, Mokrowiecka A, Jacenik D, Krajewska WM, et al.
931 Colonic Inflammation Induces Changes in Glucose Levels through Modulation of Incretin System.
932 *Pharmacol Rep* (2021) 73(6):1670-9. Epub 20210917. doi: 10.1007/s43440-021-00327-y.

933 35. Kong L, Pokatayev V, Lefkovith A, Carter GT, Creasey EA, Krishna C, et al. The Landscape
934 of Immune Dysregulation in Crohn's Disease Revealed through Single-Cell Transcriptomic Profiling
935 in the Ileum and Colon. *Immunity* (2023) 56(2):444-58 e5. Epub 20230130. doi:
936 10.1016/j.immuni.2023.01.002.

937 36. Metwaly A, Jovic J, Waldschmitt N, Khaloian S, Heimes H, Hacker D, et al. Diet Prevents
938 the Expansion of Segmented Filamentous Bacteria and Ileo-Colonic Inflammation in a Model of
939 Crohn's Disease. *Microbiome* (2023) 11(1):66. Epub 20230331. doi: 10.1186/s40168-023-01508-y.

940 37. Yoon H, Schaubeck M, Lagkouvardos I, Blesl A, Heinzlmeir S, Hahne H, et al. Increased
941 Pancreatic Protease Activity in Response to Antibiotics Impairs Gut Barrier and Triggers Colitis. *Cell*
942 *Mol Gastroenterol Hepatol* (2018) 6(3):370-88 e3. Epub 20180529. doi:
943 10.1016/j.jcmgh.2018.05.008.

944 38. Waldschmitt N, Berger E, Rath E, Sartor RB, Weigmann B, Heikenwalder M, et al. C/Ebp
945 Homologous Protein Inhibits Tissue Repair in Response to Gut Injury and Is Inversely Regulated
946 with Chronic Inflammation. *Mucosal Immunol* (2014) 7(6):1452-66. Epub 20140521. doi:
947 10.1038/mi.2014.34.

948 39. Schaubeck M, Clavel T, Calasan J, Lagkouvardos I, Haange SB, Jehmlich N, et al. Dysbiotic
949 Gut Microbiota Causes Transmissible Crohn's Disease-Like Ileitis Independent of Failure in
950 Antimicrobial Defence. *Gut* (2016) 65(2):225-37. doi: 10.1136/gutjnl-2015-309333.

951 40. Keubler LM, Buettner M, Hager C, Bleich A. A Multihit Model: Colitis Lessons from the
952 Interleukin-10-Deficient Mouse. *Inflamm Bowel Dis* (2015) 21(8):1967-75. doi:
953 10.1097/MIB.0000000000000468.

954 41. Eri R, McGuckin MA, Wadley R. T Cell Transfer Model of Colitis: A Great Tool to Assess
955 the Contribution of T Cells in Chronic Intestinal Inflammation. *Methods Mol Biol* (2012) 844:261-
956 75. doi: 10.1007/978-1-61779-527-5_19.

957 42. Crepin VF, Collins JW, Habibzay M, Frankel G. Citrobacter Rodentium Mouse Model of
958 Bacterial Infection. *Nat Protoc* (2016) 11(10):1851-76. Epub 20160908. doi:
959 10.1038/nprot.2016.100.

960 43. Jenkins BR, Blaseg NA, Grifka-Walk HM, Deuling B, Swain SD, Campbell EL, et al. Loss of
961 Interleukin-10 Receptor Disrupts Intestinal Epithelial Cell Proliferation and Skews Differentiation
962 Towards the Goblet Cell Fate. *FASEB J* (2021) 35(6):e21551. doi: 10.1096/fj.202002369R.

963 44. Fothergill LJ, Furness JB. Diversity of Enteroendocrine Cells Investigated at Cellular and
964 Subcellular Levels: The Need for a New Classification Scheme. *Histochem Cell Biol* (2018)
965 150(6):693-702. Epub 20181024. doi: 10.1007/s00418-018-1746-x.

966 45. Gehart H, van Es JH, Hamer K, Beumer J, Kretzschmar K, Dekkers JF, et al. Identification of
967 Enteroendocrine Regulators by Real-Time Single-Cell Differentiation Mapping. *Cell* (2019)
968 176(5):1158-73 e16. Epub 20190131. doi: 10.1016/j.cell.2018.12.029.

969 46. Nwako JG, McCauley HA. Enteroendocrine Cells Regulate Intestinal Homeostasis and
970 Epithelial Function. *Mol Cell Endocrinol* (2024) 593:112339. Epub 20240805. doi:
971 10.1016/j.mce.2024.112339.

972 47. Kanke M, Kennedy Ng MM, Connelly S, Singh M, Schaner M, Shanahan MT, et al. Single-
973 Cell Analysis Reveals Unexpected Cellular Changes and Transposon Expression Signatures in the
974 Colonic Epithelium of Treatment-Naive Adult Crohn's Disease Patients. *Cell Mol Gastroenterol*
975 *Hepatol* (2022) 13(6):1717-40. Epub 20220212. doi: 10.1016/j.jcmgh.2022.02.005.

976 48. Erben U, Loddenkemper C, Doerfel K, Spieckermann S, Haller D, Heimesaat MM, et al. A
977 Guide to Histomorphological Evaluation of Intestinal Inflammation in Mouse Models. *Int J Clin Exp*
978 *Pathol* (2014) 7(8):4557-76. Epub 20140715.

979 49. Jenny M, Uhl C, Roche C, Duluc I, Guillermin V, Guillemot F, et al. Neurogenin3 Is
980 Differentially Required for Endocrine Cell Fate Specification in the Intestinal and Gastric
981 Epithelium. *EMBO J* (2002) 21(23):6338-47. doi: 10.1093/emboj/cdf649.

982 50. Piccand J, Vagne C, Blot F, Meunier A, Beucher A, Strasser P, et al. Rfx6 Promotes the
983 Differentiation of Peptide-Secreting Enteroendocrine Cells While Repressing Genetic Programs
984 Controlling Serotonin Production. *Mol Metab* (2019) 29:24-39. Epub 20190813. doi:
985 10.1016/j.molmet.2019.08.007.

986 51. Okumura M, Hamada A, Ohsaka F, Tsuruta T, Hira T, Sonoyama K. Expression of Serotonin
987 Receptor Htr4 in Glucagon-Like Peptide-1-Positive Enteroendocrine Cells of the Murine Intestine.
988 *Pflugers Arch* (2020) 472(10):1521-32. Epub 20200901. doi: 10.1007/s00424-020-02453-7.

989 52. Lund ML, Egerod KL, Engelstoft MS, Dmytriyeva O, Theodorsson E, Patel BA, et al.
990 Enterochromaffin 5-Ht Cells - a Major Target for Glp-1 and Gut Microbial Metabolites. *Mol Metab*
991 (2018) 11:70-83. Epub 20180310. doi: 10.1016/j.molmet.2018.03.004.

992 53. Lund ML, Sorrentino G, Egerod KL, Kroone C, Mortensen B, Knop FK, et al. L-Cell
993 Differentiation Is Induced by Bile Acids through Gpbar1 and Paracrine Glp-1 and Serotonin
994 Signaling. *Diabetes* (2020) 69(4):614-23. Epub 20200210. doi: 10.2337/db19-0764.

995 54. Sharma D, Verma S, Vaidya S, Kalia K, Tiwari V. Recent Updates on Glp-1 Agonists:
996 Current Advancements & Challenges. *Biomed Pharmacother* (2018) 108:952-62. Epub 20180927.
997 doi: 10.1016/j.biopha.2018.08.088.

998 55. Holst JJ. The Physiology of Glucagon-Like Peptide 1. *Physiol Rev* (2007) 87(4):1409-39. doi:
999 10.1152/physrev.00034.2006.

1000 56. Ingersoll SA, Ayyadurai S, Charania MA, Laroui H, Yan Y, Merlin D. The Role and
1001 Pathophysiological Relevance of Membrane Transporter Pept1 in Intestinal Inflammation and
1002 Inflammatory Bowel Disease. *Am J Physiol Gastrointest Liver Physiol* (2012) 302(5):G484-92. doi:
1003 10.1152/ajpgi.00477.2011.

1004 57. Ogura Y, Bonen DK, Inohara N, Nicolae DL, Chen FF, Ramos R, et al. A Frameshift
1005 Mutation in Nod2 Associated with Susceptibility to Crohn's Disease. *Nature* (2001) 411(6837):603-
1006 6. doi: 10.1038/35079114.

1007 58. Zucchelli M, Torkvist L, Bresso F, Halfvarson J, Hellquist A, Anedda F, et al. Pept1
1008 Oligopeptide Transporter (Slc15a1) Gene Polymorphism in Inflammatory Bowel Disease. *Inflamm*
1009 *Bowel Dis* (2009) 15(10):1562-9. doi: 10.1002/ibd.20963.

1010 59. Lebrun LJ, Lenaerts K, Kiers D, Pais de Barros JP, Le Guern N, Plesnik J, et al.
1011 Enteroendocrine L Cells Sense Lps after Gut Barrier Injury to Enhance Glp-1 Secretion. *Cell Rep*
1012 (2017) 21(5):1160-8. doi: 10.1016/j.celrep.2017.10.008.

1013 60. Petersen N, Reimann F, Bartfeld S, Farin HF, Ringnalda FC, Vries RG, et al. Generation of L
1014 Cells in Mouse and Human Small Intestine Organoids. *Diabetes* (2014) 63(2):410-20. Epub
1015 20131015. doi: 10.2337/db13-0991.

1016 61. Smirnova MG, Guo L, Birchall JP, Pearson JP. Lps up-Regulates Mucin and Cytokine Mrna
1017 Expression and Stimulates Mucin and Cytokine Secretion in Goblet Cells. *Cell Immunol* (2003)
1018 221(1):42-9. doi: 10.1016/s0008-8749(03)00059-5.

1019 62. Delmotte P, Marin Mathieu N, Sieck GC. Tnfalpha Induces Mitochondrial Fragmentation and
1020 Biogenesis in Human Airway Smooth Muscle. *Am J Physiol Lung Cell Mol Physiol* (2021)
1021 320(1):L137-L51. Epub 20201104. doi: 10.1152/ajplung.00305.2020.

1022 63. Shinde A, Jung H, Lee H, Singh K, Roy M, Gohel D, et al. Tnf-Alpha Differentially
1023 Modulates Subunit Levels of Respiratory Electron Transport Complexes of Er/Pr +Ve/-Ve Breast
1024 Cancer Cells to Regulate Mitochondrial Complex Activity and Tumorigenic Potential. *Cancer Metab*
1025 (2021) 9(1):19. Epub 20210429. doi: 10.1186/s40170-021-00254-9.

1026 64. Berger E, Rath E, Yuan D, Waldschmitt N, Khaloian S, Allgauer M, et al. Mitochondrial
1027 Function Controls Intestinal Epithelial Stemness and Proliferation. *Nat Commun* (2016) 7:13171. doi:
1028 10.1038/ncomms13171.

1029 65. Urbauer E, Aguanno D, Mindermann N, Omer H, Metwaly A, Krammel T, et al.
1030 Mitochondrial Perturbation in the Intestine Causes Microbiota-Dependent Injury and Gene
1031 Signatures Discriminative of Inflammatory Disease. *Cell Host Microbe* (2024) 32(8):1347-64 e10.
1032 Epub 20240715. doi: 10.1016/j.chom.2024.06.013.

1033 66. Martin FP, Rezzi S, Philippe D, Tornier L, Messlik A, Holzlwimmer G, et al. Metabolic
1034 Assessment of Gradual Development of Moderate Experimental Colitis in Il-10 Deficient Mice. *J*
1035 *Proteome Res* (2009) 8(5):2376-87. doi: 10.1021/pr801006e.

1036 67. Deleyto-Seldas N, Efeyan A. The Mtor-Autophagy Axis and the Control of Metabolism.
1037 *Front Cell Dev Biol* (2021) 9:655731. Epub 20210701. doi: 10.3389/fcell.2021.655731.

1038 68. Ip WKE, Hoshi N, Shouval DS, Snapper S, Medzhitov R. Anti-Inflammatory Effect of Il-10
1039 Mediated by Metabolic Reprogramming of Macrophages. *Science* (2017) 356(6337):513-9. doi:
1040 10.1126/science.aal3535.

1041 69. Urbauer E. Mitochondrial Function in the Regulation of Epithelial Cell Homeostasis – Impact
1042 on Intestinal Pathologies: Technische Universität München (2024).

1043 70. Becker C, Kukat A, Szczepanowska K, Hermans S, Senft K, Brandscheid CP, et al. Clpp
1044 Deficiency Protects against Metabolic Syndrome but Hinders Adaptive Thermogenesis. *EMBO Rep*
1045 (2018) 19(5). Epub 20180327. doi: 10.15252/embr.201745126.

1046 71. Bhaskaran S, Pharaoh G, Ranjit R, Murphy A, Matsuzaki S, Nair BC, et al. Loss of
1047 Mitochondrial Protease Clpp Protects Mice from Diet-Induced Obesity and Insulin Resistance.
1048 *EMBO Rep* (2018) 19(3). Epub 20180202. doi: 10.15252/embr.201745009.

1049 72. Panaro BL, Yusta B, Matthews D, Koehler JA, Song Y, Sandoval DA, et al. Intestine-
1050 Selective Reduction of Gcg Expression Reveals the Importance of the Distal Gut for Glp-1 Secretion.
1051 *Mol Metab* (2020) 37:100990. Epub 20200409. doi: 10.1016/j.molmet.2020.100990.

1052 73. Wichmann A, Allahyar A, Greiner TU, Plovier H, Lunden GO, Larsson T, et al. Microbial
1053 Modulation of Energy Availability in the Colon Regulates Intestinal Transit. *Cell Host Microbe*
1054 (2013) 14(5):582-90. doi: 10.1016/j.chom.2013.09.012.

1055 74. Karhunen LJ, Juvonen KR, Huotari A, Purhonen AK, Herzig KH. Effect of Protein, Fat,
1056 Carbohydrate and Fibre on Gastrointestinal Peptide Release in Humans. *Regul Pept* (2008) 149(1-
1057 3):70-8. Epub 20080325. doi: 10.1016/j.regpep.2007.10.008.

1058 75. Kaelberer MM, Rupprecht LE, Liu WW, Weng P, Bohorquez DV. Neuropod Cells: The
1059 Emerging Biology of Gut-Brain Sensory Transduction. *Annu Rev Neurosci* (2020) 43:337-53. Epub
1060 20200226. doi: 10.1146/annurev-neuro-091619-022657.

1061 76. Bohorquez DV, Shahid RA, Erdmann A, Kreger AM, Wang Y, Calakos N, et al.
1062 Neuroepithelial Circuit Formed by Innervation of Sensory Enteroendocrine Cells. *J Clin Invest*
1063 (2015) 125(2):782-6. Epub 20150102. doi: 10.1172/JCI78361.

1064 77. Barton JR, Londregan AK, Alexander TD, Entezari AA, Covarrubias M, Waldman SA.
1065 Enteroendocrine Cell Regulation of the Gut-Brain Axis. *Front Neurosci* (2023) 17:1272955. Epub
1066 20231107. doi: 10.3389/fnins.2023.1272955.

1067 78. Abbott CR, Monteiro M, Small CJ, Sajedi A, Smith KL, Parkinson JR, et al. The Inhibitory
1068 Effects of Peripheral Administration of Peptide Yy(3-36) and Glucagon-Like Peptide-1 on Food
1069 Intake Are Attenuated by Ablation of the Vagal-Brainstem-Hypothalamic Pathway. *Brain Res* (2005)
1070 1044(1):127-31. Epub 20050407. doi: 10.1016/j.brainres.2005.03.011.

1071 79. Brierley DI, de Lartigue G. Reappraising the Role of the Vagus Nerve in Glp-1-Mediated
1072 Regulation of Eating. *Br J Pharmacol* (2022) 179(4):584-99. Epub 20210731. doi:
1073 10.1111/bph.15603.

1074 80. Lu VB, Rievaj J, O'Flaherty EA, Smith CA, Pais R, Pattison LA, et al. Adenosine
1075 Triphosphate Is Co-Secreted with Glucagon-Like Peptide-1 to Modulate Intestinal Enterocytes and
1076 Afferent Neurons. *Nat Commun* (2019) 10(1):1029. Epub 20190304. doi: 10.1038/s41467-019-
1077 09045-9.

1078 81. Nguyen AT, Mandard S, Dray C, Deckert V, Valet P, Besnard P, et al. Lipopolysaccharides-
1079 Mediated Increase in Glucose-Stimulated Insulin Secretion: Involvement of the Glp-1 Pathway.
1080 *Diabetes* (2014) 63(2):471-82. doi: 10.2337/db13-0903.

1081 82. Williams L, Alshehri A, Robichaud B, Cudmore A, Gagnon J. The Role of the Bacterial
1082 Muramyl Dipeptide in the Regulation of Glp-1 and Glycemia. *Int J Mol Sci* (2020) 21(15). Epub
1083 20200724. doi: 10.3390/ijms21155252.

1084 83. Gribble FM, Reimann F. Enteroendocrine Cells: Chemosensors in the Intestinal Epithelium.
1085 *Annual review of physiology* (2016) 78:277-99. Epub 2015/10/08. doi: 10.1146/annurev-physiol-
1086 021115-105439.

1087 84. Gagnon J, Sauve M, Zhao W, Stacey HM, Wiber SC, Bolz SS, et al. Chronic Exposure to
1088 Tnfalpha Impairs Secretion of Glucagon-Like Peptide-1. *Endocrinology* (2015) 156(11):3950-60.
1089 Epub 2015/08/14. doi: 10.1210/en.2015-1361.

1090 85. Selleri S, Palazzo M, Deola S, Wang E, Balsari A, Marincola FM, et al. Induction of Pro-
1091 Inflammatory Programs in Enteroendocrine Cells by the Toll-Like Receptor Agonists Flagellin and
1092 Bacterial Lps. *International immunology* (2008) 20(8):961-70. Epub 2008/06/12. doi:
1093 10.1093/intimm/dxn055.

1094 86. Bogunovic M, Dave SH, Tilstra JS, Chang DT, Harpaz N, Xiong H, et al. Enteroendocrine
1095 Cells Express Functional Toll-Like Receptors. *Am J Physiol Gastrointest Liver Physiol* (2007)
1096 292(6):G1770-83. doi: 10.1152/ajpgi.00249.2006.

1097 87. Wong CK, Yusta B, Koehler JA, Baggio LL, McLean BA, Matthews D, et al. Divergent
1098 Roles for the Gut Intraepithelial Lymphocyte Glp-1r in Control of Metabolism, Microbiota, and T
1099 Cell-Induced Inflammation. *Cell Metab* (2022) 34(10):1514-31 e7. Epub 20220825. doi:
1100 10.1016/j.cmet.2022.08.003.

1101 88. Habib AM, Richards P, Cairns LS, Rogers GJ, Bannon CA, Parker HE, et al. Overlap of
1102 Endocrine Hormone Expression in the Mouse Intestine Revealed by Transcriptional Profiling and
1103 Flow Cytometry. *Endocrinology* (2012) 153(7):3054-65. Epub 2012/06/12. doi: 10.1210/en.2011-
1104 2170.

1105 89. Egerod KL, Engelstoft MS, Grunddal KV, Nohr MK, Secher A, Sakata I, et al. A Major
1106 Lineage of Enteroendocrine Cells Coexpress Cck, Secretin, Gip, Glp-1, Pyy, and Neurotensin but
1107 Not Somatostatin. *Endocrinology* (2012) 153(12):5782-95. Epub 2012/10/16. doi: 10.1210/en.2012-
1108 1595.

1109 90. Sykaras AG, Demenis C, Cheng L, Pisitkun T, McLaughlin JT, Fenton RA, et al. Duodenal
1110 Cck Cells from Male Mice Express Multiple Hormones Including Ghrelin. *Endocrinology* (2014)
1111 155(9):3339-51. Epub 2014/07/09. doi: 10.1210/en.2013-2165.

1112 91. Drucker DJ, Habener JF, Holst JJ. Discovery, Characterization, and Clinical Development of
1113 the Glucagon-Like Peptides. *J Clin Invest* (2017) 127(12):4217-27. Epub 20171201. doi:
1114 10.1172/JCI97233.

1115 92. Lee SJ, Lee J, Li KK, Holland D, Maughan H, Guttman DS, et al. Disruption of the Murine
1116 Glp2r Impairs Paneth Cell Function and Increases Susceptibility to Small Bowel Enteritis.
1117 *Endocrinology* (2012) 153(3):1141-51. doi: 10.1210/en.2011-1954.

1118 93. Qi KK, Wu J, Wan J, Men XM, Xu ZW. Purified Pegylated Porcine Glucagon-Like Peptide-2
1119 Reduces the Severity of Colonic Injury in a Murine Model of Experimental Colitis. *Peptides* (2014)
1120 52:11-8. doi: 10.1016/j.peptides.2013.11.012.

1121 94. Boushey RP, Yusta B, Drucker DJ. Glucagon-Like Peptide 2 Decreases Mortality and
1122 Reduces the Severity of Indomethacin-Induced Murine Enteritis. *Am J Physiol* (1999) 277(5 Pt
1123 1):E937-47.

1124 95. Alavi K, Schwartz MZ, Palazzo JP, Prasad R. Treatment of Inflammatory Bowel Disease in a
1125 Rodent Model with the Intestinal Growth Factor Glucagon-Like Peptide-2. *J Pediatr Surg* (2000)
1126 35(6):847-51. doi: 10.1053/jpsu.2000.6861.

1127 96. Drucker DJ, Yusta B, Boushey RP, DeForest L, Brubaker PL. Human [Gly2]Glp-2 Reduces
1128 the Severity of Colonic Injury in a Murine Model of Experimental Colitis. *Am J Physiol* (1999) 276(1
1129 Pt 1):G79-91.

1130 97. Buchman AL, Katz S, Fang JC, Bernstein CN, Abou-Assi SG, Teduglutide Study G.
1131 Teduglutide, a Novel Mucosally Active Analog of Glucagon-Like Peptide-2 (Glp-2) for the
1132 Treatment of Moderate to Severe Crohn's Disease. *Inflamm Bowel Dis* (2010) 16(6):962-73. doi:
1133 10.1002/ibd.21117.

1134 98. Urbauer E, Aguanno D, Mindermann N, Omer H, Metwaly A, Krammel T, et al.
1135 Mitochondrial Perturbation in the Intestine Causes Microbiota-Dependent Injury and Gene
1136 Signatures Discriminative of Inflammatory Disease. *bioRxiv* (2024):2023.07.27.549844. doi:
1137 10.1101/2023.07.27.549844.

1138 99. Huang C, Wang J, Liu H, Huang R, Yan X, Song M, et al. Ketone Body Beta-
1139 Hydroxybutyrate Ameliorates Colitis by Promoting M2 Macrophage Polarization through the Stat6-
1140 Dependent Signaling Pathway. *BMC Med* (2022) 20(1):148. Epub 20220415. doi: 10.1186/s12916-
1141 022-02352-x.

1142 100. Weber-Stiehl S, Taubenheim J, Jarke L, Rocken C, Schreiber S, Aden K, et al. Hexokinase 2
1143 Expression in Apical Enterocytes Correlates with Inflammation Severity in Patients with
1144 Inflammatory Bowel Disease. *BMC Med* (2024) 22(1):490. Epub 20241023. doi: 10.1186/s12916-
1145 024-03710-7.

1146 101. Tu1826 Impact of Glp-1 Receptor Agonist on Clinical Outcomes in Patients with Crohn's
1147 Disease and Ulcerative Colitis: Insights from a Large-Scale Cohort Study. *Gastroenterology* (2024)
1148 166(5, Supplement):S-1424-S-5. doi: https://doi.org/10.1016/S0016-5085(24)03727-2.

1149 102. Rath E, Berger E, Messlik A, Nunes T, Liu B, Kim SC, et al. Induction of Dsrna-Activated
1150 Protein Kinase Links Mitochondrial Unfolded Protein Response to the Pathogenesis of Intestinal
1151 Inflammation. *Gut* (2011). Epub 2011/10/15. doi: 10.1136/gutjnl-2011-300767.

1152 103. Seiferling D, Szczepanowska K, Becker C, Senft K, Hermans S, Maiti P, et al. Loss of Clpp
1153 Alleviates Mitochondrial Cardiomyopathy without Affecting the Mammalian Uprmt. *EMBO Rep*
1154 (2016) 17(7):953-64. Epub 20160506. doi: 10.15252/embr.201642077.

1155 104. Lamas B, Michel ML, Waldschmitt N, Pham HP, Zacharioudaki V, Dupraz L, et al. Card9
1156 Mediates Susceptibility to Intestinal Pathogens through Microbiota Modulation and Control of
1157 Bacterial Virulence. *Gut* (2018) 67(10):1836-44. Epub 20170808. doi: 10.1136/gutjnl-2017-314195.

1158 105. Zietek T, Rath E. Chapter 3 - Intestinal Organoids: Mini-Guts Grown in the Laboratory. In:
1159 Davies JA, Lawrence ML, editors. *Organs and Organoids*. Academic Press (2018). p. 43-71.

1160 106. Zietek T, Giesbertz P, Ewers M, Reichart F, Weinmuller M, Urbauer E, et al. Organoids to
1161 Study Intestinal Nutrient Transport, Drug Uptake and Metabolism - Update to the Human Model and
1162 Expansion of Applications. *Front Bioeng Biotechnol* (2020) 8:577656. Epub 20200911. doi:
1163 10.3389/fbioe.2020.577656.

1164 107. Zietek T, Rath E, Haller D, Daniel H. Intestinal Organoids for Assessing Nutrient Transport,
1165 Sensing and Incretin Secretion. *Sci Rep* (2015) 5:16831. doi: 10.1038/srep16831.

1166